

Influences of Thermal Annealing on Physical Properties of Graphene Nanoplatelets



Thesis

M.S Physics

By

Muhammad Akhtar

Reg. No. 157-FBAS/MSPHY/S13

Supervised by

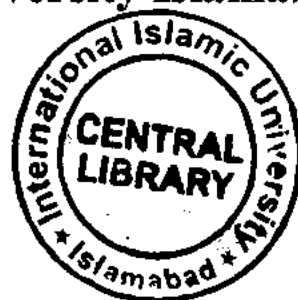
Dr. Javed Iqbal Saggu

Department of Physics

Faculty of Basic and Applied Sciences

International Islamic University Islamabad

(2015)



Accession No TH 15200

MS

620.5

MU1

nanosstructure materials

nanotechnology

Certificate

This is to certify that the work contained in this thesis entitled: “**Influences of Thermal Annealing on Physical Properties of Graphene Nanoplatelets**” has been carried out by **Muhammad Akhtar (157-FBAS/MSPHY/S13)** in Laboratory of Nanoscience and Technology (LNT) under my supervision. In my opinion, this is fully adequate in scope and quality for the degree of Master of Sciences (MS) in Physics.


Supervisor **Dr. Javed Iqbal Saggu**
Assistant Professor (Physics)
International Islamic University
Islamabad.

Dr. Javed Iqbal Saggu

Department of Physics

International Islamic University, Islamabad.

Influences of Thermal Annealing on Physical Properties of Graphene Nanoplatelets

By

Muhammad Akhtar

157-FBAS/MSPHY/S13

A thesis submitted to

Department of Physics

For the award of the degree of

MS Physics

Signature: _____



CHAIRMAN
DEPT. OF PHYSICS

(Chairman, Department of Physics, IIU)

International Physics High
Islamabad



Signature: _____

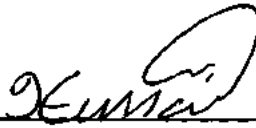
(Dean FBAS, IIU, Islamabad)

FINAL APPROVAL

It is certified that the work presented in this thesis entitled “**Influences of Thermal Annealing on Physical Properties of Graphene Nanoplatelets**” by Mr. Muhammad Akhtar bearing Registration No. 157-FBAS/MSPHY/S13 is of sufficient standard in scope and quality for the award of degree of MS Physics from International Islamic University, Islamabad.

COMMITTEE

External Examiner



Dr. Iftikhar Hussain Gul

School of Chemical and Materials Engineering (SCME),

NUST, H-12, Islamabad.

Internal Examiner



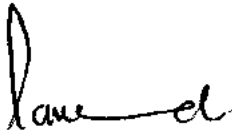
Dr. Waqar Adil Syed (Chairman)

Department of Physics

FBAS, IIUI

CHAIRMAN
DEPT. OF PHYSICS
International Islamic University
Islamabad

Supervisor



Dr. Javed Iqbal Saggu

Department of Physics,

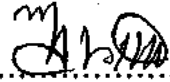
FBAS, IIUI

Dr. Javed Iqbal Saggu
Assistant Professor (Physics)
International Islamic University
Islamabad

بِسْمِ اللَّهِ الرَّحْمَنِ الرَّحِيمِ

Declaration

I hereby declare that this thesis work, neither as a whole nor a part of it has been copied out from any source. Further, work presented in this dissertation has not been submitted in support of any application for any other degree or qualification to any other university or institute and is considerable under the plagiarism rules of Higher Education Commission (HEC), Pakistan. Plagiarism report is generated by software turnitin through ID 588392501 with similarity index 06%. I also declare that If there is any plagiarism in the thesis, I, Muhammad Akhtar myself will be responsible.

Signature: 

Name: Muhammad akhtar

Reg. No: 157-FBAS/MSPHY/S13

Dedicated

To

My Parents

And

All Respected Teachers

Acknowledgement

All praises and thanks are for ALMIGHTY ALLAH, The Most Merciful, Compassionate, Gracious and Beneficent who is entire source of all knowledge and wisdom endowed to mankind. I offer my humble thank to the Holy Prophet MUHAMMAD (Sallallahu *Alaihi Wa Sallam*), who is forever a model of guidance and knowledge for humanity.

The work in this thesis could not have been accomplished without the contribution of guidance, support and friendship of many people. First of all, great gratitude should be extended to my supervisor, **Dr. Javed Iqbal Saggu**, Assistance Professor, Department of Physics IIUI, for his kind supervision, keen interest, valuable guidance and helpful technical support throughout my PhD study. His wide knowledge, logical way of thinking, constant encouragement and timely guidance provided a good basis for the thesis. His observations and comments helped me to establish the overall direction of the research and to move ahead.

I am thankful to the entire academic and administrative staff of the Department of Physics, IIUI. I am also grateful to Dr. Iftikhar H. Gul (NUST), Dr. Muhammad Saifullah Awan (ISIT) and Rashda Abbasi (IBGE) and Dr. Asma Gul (IIU) for helping and providing access to different characterization facilities.

I am glad that I have so many considerate and supportive lab mates. My special gratitude to Mr. Muhammad Saleem, Mr. Tariq Jan, Mr. Fazal Abbas, Mr. Umar Farooq, Muhammad Umair Ali, Ms. Aqsa Arshad, Mr. Asghar Ali, Mr. Faisal, Mr. Waheed Ahmad and all other members of Laboratory of Nanoscience and Technology (LNT) for the pleasant moments experienced during my study. Their suggestions and support helped me to improve my presentation skills. I am also grateful to everyone else of my friends for their deep concern and enthusiastic support. My heartiest gratitude goes to my parents for supporting me under any circumstances. Their continuous guidance and support has helped me to evolve as a good human. Last but not least, I would like to thank my wife, and daughter to be on my side always. Without their help, I would have faced many difficulties while completing my thesis.

Muhammad Akhtar

Table of Contents

CHAPTER NO.1	1
1 INTRODUCTION	1
1.1 Nano-Materials	1
1.2 Nanostructured Carbon Materials	1
1.2.1 What is Carbon?	1
1.2.2 Physical Properties of Carbon	2
1.2.3 Carbon Structure and Isotopes	2
1.2.4 Hybridization in Carbon.....	4
1.2.5 Carbon Allotropes	6
1.2.6 Carbon-based Nanostructure Materials	10
1.2.7 Carbon Nanostructured Materials of Different Dimensionalities	11
1.3 Graphene	14
1.3.1 Electronic Structure and Bonding of Graphene	15
1.3.2 Why Graphene is Important?	17
1.3.3 Single, Double and Multilayer Graphene.....	17
1.4 Graphene Nano-Platelets (GNPs): Our material of interest	19
1.4.1 Why Graphene Nanoplatelets are Important?	19
1.4.2 Characteristics of Graphene Nanoplatelets (GNPs)	20
1.4.3 Applications of Graphene Nanoplatelets.....	20
1.5 Heat Treatment	21
1.5.1 Thermal Annealing.....	22
1.5.2 Recovery, Recrystallization and Grain Growth	22
CHAPTER NO.2	24
2 MATERIAL AND METHODS	24
2.1 Sample Preparation	24
2.1.1 Procedure.....	24
2.2 Vacuum Annealing of Prepared Samples	24
CHAPTER NO.3	26
3 CHARACTERIZATION TECHNIQUES	26
3.1 X-Ray Diffraction (XRD)	26
3.1.1 Working.....	26
3.1.2 Bragg's Law	27

3.2	Microscopic Studies	28
3.2.1	Scanning Electron Microscopy	28
3.2.2	Energy Dispersive X-Ray Spectroscopy (EDS or EDX)	29
3.2.3	Transmission Electron Microscopy.....	31
3.3	Raman Spectroscopy	31
3.3.1	What is Raman Effect?.....	31
3.3.2	Elastic Rayleigh Scattering	32
3.3.3	Raman in-elastic Scattering.....	32
3.4	Dielectric Properties Measurements	35
3.4.1	What is LCR meter?	35
3.4.2	Measurement Principle.....	36
3.4.3	Working of LCR meter.....	37
CHAPTER NO.4		38
4	RESULTS AND DISCUSSIONS	38
4.1	Structural Analysis	38
4.1.1	Calculation of FWHM, d-spacing, grain size, and number of layers	39
4.2	Analysis of Raman Spectra	42
4.3	Morphology of Graphene Nanoplatelets	45
4.3.1	EDX analysis.....	46
4.4	Measurement of Dielectric Properties	47
4.4.1	Variation in dielectric constant with frequency	47
4.4.2	Variation in dielectric constant with temperature	48
4.4.3	Variation in dielectric loss with frequency and temperature.....	49
4.4.4	Variation in Dielectric loss tangent with frequency and temperature	51
4.4.5	Variation in A.C conductivity with frequency	52
4.4.6	Variation in A.C conductivity with temperature (defects)	53
5	CONCLUSIONS	55
6	REFERENCES	56
7	TURNITIN REPORT	63

List of Figures

Figure 1-1: Natural isotopes of carbon [5].....	3
Figure 1-2: Electronic configuration of carbon atom [5].....	4
Figure 1-3: sp^3 Hybridization [7].....	4
Figure 1-4: sp^2 Hybridization [7].....	5
Figure 1-5: sp Hybridization [7].....	5
Figure 1-6: Different allotropic forms of carbon [8].....	6
Figure 1-7: Three dimensional structure of graphite [10].....	7
Figure 1-8: Arrangement of layers in hexagonal and rhombohedral graphite [12].....	8
Figure 1-9: Diamond and its crystal structure [14].....	8
Figure 1-10: Ball & stick models of several amorphous carbon networks (red, blue and grey spheres are the sp^4 , sp^3 and sp^2 atoms, respectively) [17].....	10
Figure 1-11: Graphene as a basic building block for all Graphitic forms [24].....	12
Figure 1-12: Different structures of Fullerenes (a) C_{20} (b) C_{40} (c) C_{240} and (d) C_{540} [30].....	13
Figure 1-13: Different types of CNTs, Surface of (a) armchair (b) chiral CNTs, (c) Schematic presentation of Multi-Wall CNT [30].....	14
Figure 1-14: Isolation of graphene from graphite [33].....	15
Figure 1-15: sp^2 hybridization in graphene [36].....	16
Figure 1-16: Graphene and its reciprocal lattice (a) Lattice structure of graphene, a_1 and a_2 are the lattice vectors. Graphene unit cell (shaded area) contains two carbon atoms (A and B). (b) g_1 and g_2 are the reciprocal lattice vectors of graphene. The corresponding first Brillion zone is depicted as the shaded hexagonal. The Dirac cones located at K and K' points [37].	16
Figure 1-17: Schematic representation of band structure of graphene with two in-equivalent k- and k'-points, at the vertex of Brillion Zone display no energy band gap between two sub lattices [38].....	16
Figure 1-18: 2D primitive cells of Graphene with different stacking sequences [46].....	18
Figure 1-19: Overview of Applications of Graphene Nanoplatelets (GNPs) [66].....	21
Figure 1-20: Grain size verses annealing temperature is shown. Grain structure during Recovery, Recrystallization and Grain Growth phases are shown schematically [67].....	23
Figure 2-1: Desk-top Powder Presser (Model YLJ-24T) [68].....	24
Figure 2-2 Block diagram of Vacuum annealing of Graphene Nanoplatelets (GNPs) [69].....	25

Figure 3-1: Main parts of X-ray Diffractometer [70]	27
Figure 3-2: Schematic diagram of Bragg's Law [71].....	28
Figure 3-3: Schematic representation of SEM and TEM, showing their main components [78]	29
Figure 3-4: EDX basic principle with EDX spectrum [82]	30
Figure 3-5: Schematic representation of an energy-dispersive spectrometer [82]	30
Figure 3-6: Block diagram of Raman and Rayleigh scattering [86].....	32
Figure 3-7: Raman Effect (Top) and (b) Raman spectrum (Bottom) [88].....	33
Figure 3-8: Raman spectra of (a) Graphene (top) and Graphite (bottom) [90]	34
Figure 3-9: Comparison of Raman spectra of HOPG graphite, mono, bi- and tri-layers graphene [90].....	34
Figure 3-10: Raman spectra of graphene for a less ordered (top) and well-ordered (bottom) structure showing how D peak grows with increasing defects [92].....	35
Figure 3-11: The 7600 Precision LCR Meter with LD-03 Dielectric Cell was designed to find Dielectric Constant and Dissipation Factor measurements [93].....	36
Figure 3-12: Principle Drawing of Automatic Balancing Bridge of LCR meter [94]	36
Figure 4-1: XRD pattern of GNPs samples (a) G-rt, (b) G300, (c) G500, (d) G700, (e) G900 and (f) G1100 annealed from 300 to 1100 °C for 1 hour in vacuum. ...	38
Figure 4-2: Extended XRD pattern of GNPs samples for (002) plane	39
Figure 4-3: Variation in d-spacing d_{002} of GNPs with increasing Temperature	41
Figure 4-4: Variation in FWHM of GNPs with increasing Temperature	41
Figure 4-5: Variation in Grain Size of GNPs with increasing Temperature.....	41
Figure 4-6: Variation in number of GNPs layers with increasing Temperature.....	42
Figure 4-7: Raman spectra of the GNPs samples annealed at 300-1100 °C, showing D, G and 2D bands.....	43
Figure 4-8: Variation in Defects (Peak intensity ratio I_D/I_G) of GNPs with increasing Temperature.....	44
Figure 4-9: FE-SEM images (a) un-annealed GNPs (b) GNPs annealed at 300°C (c) GNPs annealed at 700°C and (d) GNPs annealed at 1100 °C for 1 hour in vacuum	45
Figure 4-10: EDX spectra of (a) un-annealed GNPs (b) GNPs annealed at 300 °C (c) GNPs annealed at 700 °C and (d) GNPs annealed at 1100 °C for 1 hour in vacuum	46
Figure 4-11: Variation in dielectric constant as a function of frequency of GNPs samples annealed at 300-1100 °C	48

Figure 4-12: Variation in dielectric constant of GNPs with increasing temperature.....	49
Figure 4-13: Variation in dielectric Loss as a function of frequency of GNPs samples annealed at 300-1100 °C.....	50
Figure 4-14: Variation in Dielectric loss tangent, as a function of (a) frequency and (b) temperature of GNPs samples annealed at 300-1100 °C	51
Figure 4-15: Variation in A.C Conductivity with frequency of GNPs samples annealed at 300-1100 °C.....	52
Figure 4-16: Variation in A.C conductivity with increasing Temperature at Fixed Frequency	53

List of Tables

Table 1-1: Physical properties of carbon	2
Table 1-2: Comparison between properties of graphite and diamond.....	9
Table 1-3: Comparison between properties of graphene and carbon nanotubes	17
Table 4-1: Calculation of FWHM, d-spacing, particle size, intensity (cps) and no. of layers for (002) planes of GNPs samples.	39
Table 4-2: Calculations of peak position of D, G, 2D bands and peak intensity ratio I_D/I_G of GNPs annealed at 300-1100 °C.....	43

Abstract

The current study investigates the variation in structural, morphological, and dielectric properties of GNPs annealed at temperature ranging from 300-1100 °C under vacuum conditions. Commercially available purified GNPs powder has been used to prepare pellets of the sample. The change in physical properties of as-prepared and annealed samples of GNPs have been studied using X-ray diffraction, Field Emission Scanning Electron Microscopy, Raman spectroscopy and LCD meter.

The structural study has clearly showed the improvement in the crystallinity, enhancement in number of graphene layers and grain size by annealing. A slight shift in diffraction peak (002) toward lower and higher angles (2θ) has also been observed with corresponding change in lattice parameters for all heat treated samples. Raman spectra reveals that defects ratio (I_D/I_G) have reduced from 0.368 to 0.314 in the annealed samples up to 700 °C and then have increased abruptly from 0.314 to 0.550 above 700 °C due to breakage of C=C bond in hexagonal network of GNPs. FESEM images has displayed that during thermal annealing of GNPs, their platelet like overlapped morphology is increased by increasing temperature from 300 to 1100 °C and agglomerated with irregular boundaries. The dielectric properties of GNPs have calculated from 100Hz to 5MHz frequency range. A significant change in dielectric constant and dielectric loss at low frequency has been observed. Also at fixed frequency, dielectric constant has varied with defects while dielectric loss tangent has decreased by annealing. The AC conductivity of GNPs is found to be increased linearly with increasing frequency and then started to decrease at relatively high frequencies for all annealed samples. Similarly The AC conductivity of GNPs is considerably increased with increasing defects by annealing the samples.

These results demonstrate that this easy, environmentally-friendly and low-cost technique (vacuum thermal annealing) to improve quality of Graphene Nano platelets is reliable and promising. Therefore, it is suggested that to improve the quality of GNPs through vacuum thermal annealing, 700 °C is the optimal temperature to obtain GNPs with least defects.

To our knowledge, this is the first reported research work of this particular (GNPs) carbon nanostructured material.

CHAPTER NO.1

1 INTRODUCTION

1.1 Nano-Materials

Nanoscience concerns with synthesis, characterization, investigation and utilization of nanostructured materials. These materials have at least one length in the nanometer dimension. A nanometer (nm) is defined as one billionth part of a meter or 10^{-9} m. One nanometer length is almost corresponding to diameter of 5 silicon or 10 hydrogen atoms [1].

The structure, properties and processing of materials with grain size ranging from 10 to 100 nm are research field of main concern during the last two decades. A major revolution in medical, engineering and material sciences is going on as investigators discovery new ways to design, fabricate and techniques to identify materials at nanoscale. Novel materials with remarkable optical, mechanical, magnetic and electrical properties are speedily developed for use in environmental, energy, information technology, medicine and bioengineering applications [2].

At nanometer scale, some chemical and physical properties of the materials can fluctuate considerably from the bulk structured materials with same composition. Crystals have a low melting point and decreased lattice constants at nanometer scale, for the reason that the number of surface atoms to the total number of atoms becomes a significant and the surface energy presents a key function in the thermal stability. Therefore, many material properties must now be re-examined in view of the fact that a significant enhancement in surface/volume ratio is associated with the reduction in dimension of the material at nanometer scale, possessing a significant influence on material efficiency [3].

1.2 Nanostructured Carbon Materials

1.2.1 What is Carbon?

The word Carbon comes from Latin carbo and French charbon meaning charcoal. Carbon is simultaneously one of the hardest (diamond) and softest (graphite) material exist in nature. Carbon (by mass) is the fourth highest bountiful element in the universe after H, He, and O and the 15th most bountiful element in the Earth's crust. Carbon is also found in all living organisms and is the 2nd most bountiful element in the human body (18% of body weight) after Oxygen. In Periodic Table, it is placed in Group 14, Period 2 element and having

P Block. Sumerians and Egyptians discovered it around 3750 BC. In 1789, Carbon as an element was identified by Antoine Lavoisier [4].

1.2.2 Physical Properties of Carbon

Table 1-1: Physical properties of carbon

Physical properties of carbon	
Name	Carbon
Symbol	C
Group, period, block	14, 2, p-block
Classification	Non-metal
Phase	Solid
Atomic number	6
Electronic configuration	$1s^2, 2s^2, 2p^2$
Number of Electrons or Protons	6
Number of Neutrons	6,7,8
Atomic mass	12 amu
Isotopes	$^{12}\text{C}, ^{13}\text{C}, ^{14}\text{C}$
Allotropes	Graphite, Diamond, Graphene, Fullerene Amorphous, , Carbon nanotubes
Crystal structure	Hexagonal (Graphite), Cubic (Diamond)
Density (at room temp.)	Graphite : 2.26 g/cm^3 Diamond : 3.56 g/cm^3
Color	Grey(Graphite), Clear (Diamond)
Oxidation State	+ 4 (CCl_4) to - 4 (SiC)
Melting point (Graphite)	$3652.0 \text{ }^\circ\text{C}$
Boiling point (Graphite)	$4827.0 \text{ }^\circ\text{C}$
Refractive index	2.417 ((Diamond)
Thermal Conductivity	Diamond: $900\text{-}2300 \text{ W}\cdot\text{m}^{-1}\cdot\text{K}^{-1}$ <hr/> Graphite: $119\text{-}165 \text{ W}\cdot\text{m}^{-1}\cdot\text{K}^{-1}$

Reproduced from: www.americanelements.com

1.2.3 Carbon Structure and Isotopes

Carbon is the basic building block of graphene and graphite. It is placed at sixth position in the periodic table and contains six electrons, six protons while having different numbers (6, 7 and 8) of neutrons. Carbon having atomic number six and seven produces ^{12}C and ^{13}C as stable isotopes while atomic number eight generates ^{14}C as radioactive isotope. ^{12}C

having zero nuclear spin is the most common isotope with 99% of all C-atoms, while ^{13}C with half nuclear spin is only 1% in nature as shown in Fig.1-1.

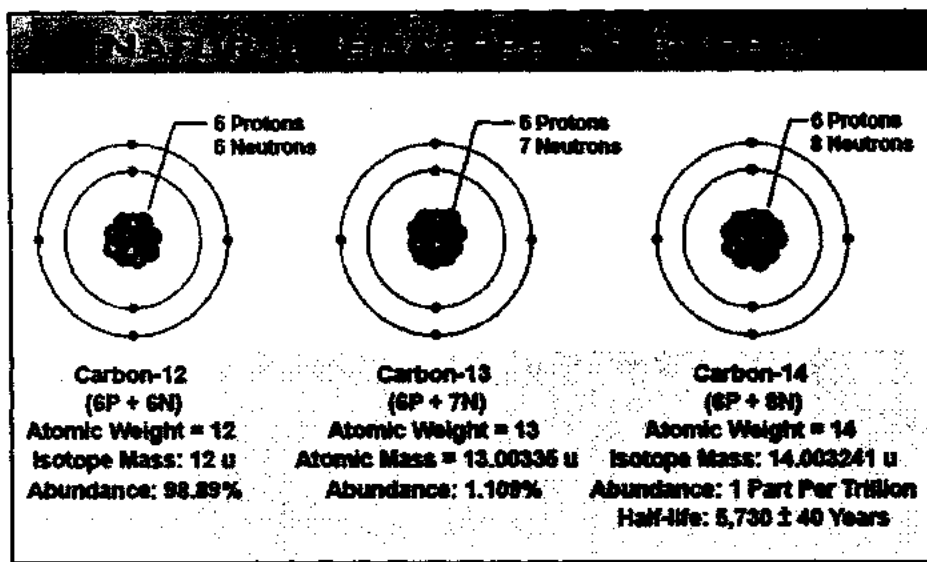


Figure 1-1: Natural isotopes of carbon [5]

^{14}C traces are extremely in trivial amount (1 part per trillion) in nature which decays in to ^{14}N emitting β^- particle. Despite ^{14}C exists in extremely small amount, it is an essential isotope studied for chronological dating. On account of its half-life of 5730 years, ^{14}C is mostly practiced to evaluate the age of dead plant or animal by calculating its absorbed amount in that dead sample. On the whole, carbon is the essential part of all organic molecules and hence, responsible for life on earth [5].

As carbon has six electrons, its electronic configuration is $1s^2 2s^2 2p^2$. First two electrons occupy 1s-orbital which is insignificant for chemical reactions due to closeness of nucleus while other four electrons fill outer 2s and 2p-orbitals. Out of four, 2 electrons occupy 2s-orbital and remain 2 electrons fill 2p-orbital. The 2p-orbital is divided in to sub-orbitals 2px, 2py, and 2pz. Out of 2, one electron fills 2px and other 2py sub-orbital while 2pz sub-orbital remains empty. The variation in energy between 2s and 2p orbitals is 4 eV. When carbon atom forms covalent bond with hydrogen, oxygen and other carbon atoms, less energy (4 eV) is required to excite 1 electron from the 2s-orbitals to the 2p-orbitals, as compared to 1s orbitals as shown in Fig.1-2.

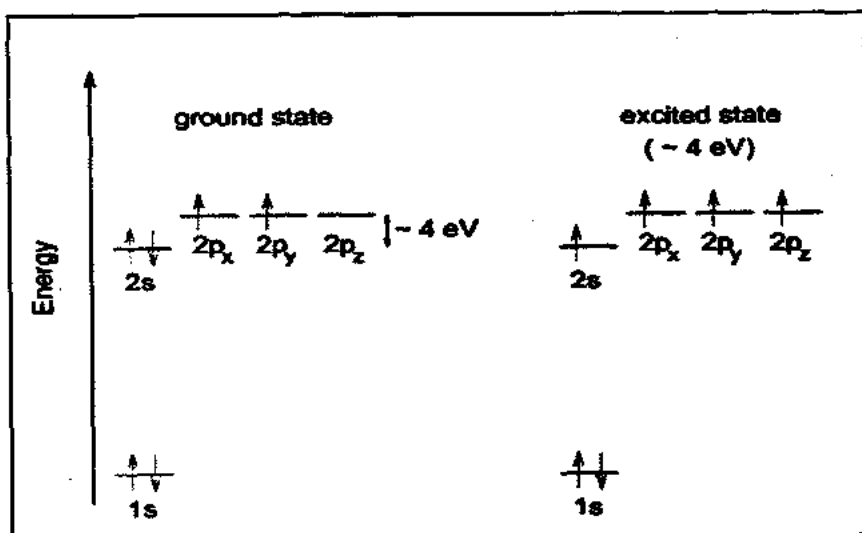


Figure 1-2: Electronic configuration of carbon atom [5]

1.2.4 Hybridization in Carbon

Orbitals of the same atom can overlap, merge and undergo a process of hybridization to form a new set of hybrid atomic orbitals that have a definite shape and orientation. In hybridization process, atomic orbitals involved yield the same the number of hybrid orbitals. These hybrid orbitals (sp , sp^2 , sp^3 , sp^3d and sp^3d^2) are mathematical models used to explain localized bonds and cannot be directly studied or measured.

Hybridization can be classified in to three categories on the basis of hybridization index.

1. **sp^3 or Tetrahedral Hybridization:** In sp^3 hybridization, one 2s and three 2p orbitals participate, following in making of four sp^3 hybridized orbitals as shown in Fig.1-3.

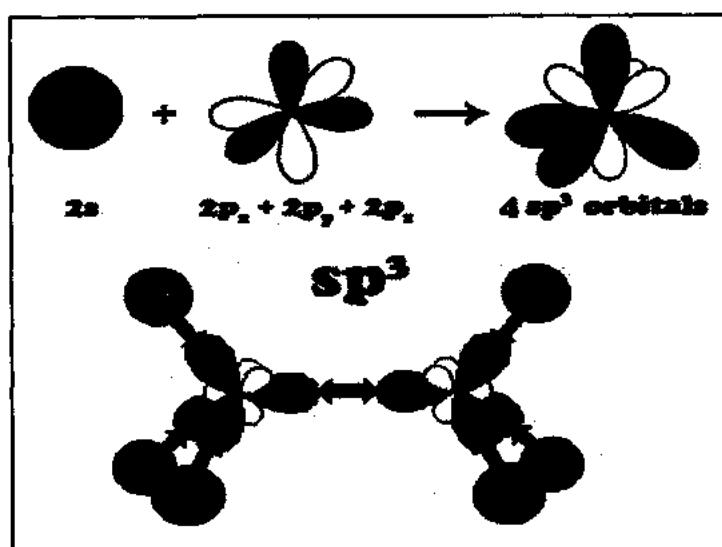


Figure 1-3: sp^3 Hybridization [7]

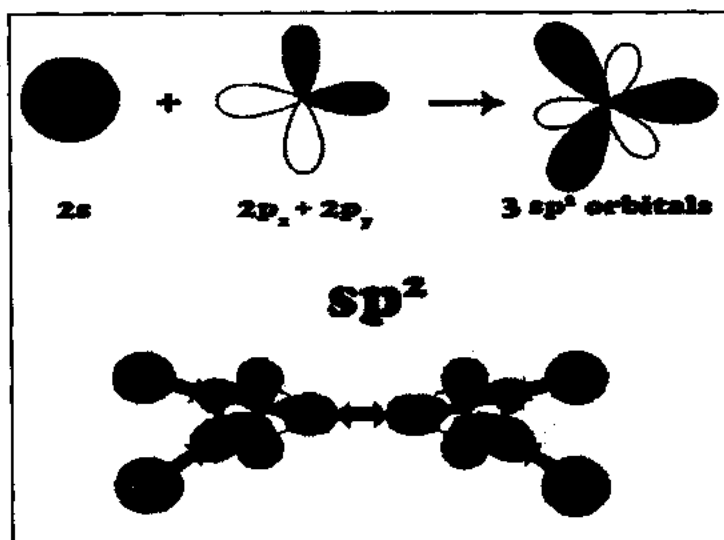


Figure 1-4: sp^2 Hybridization [7]

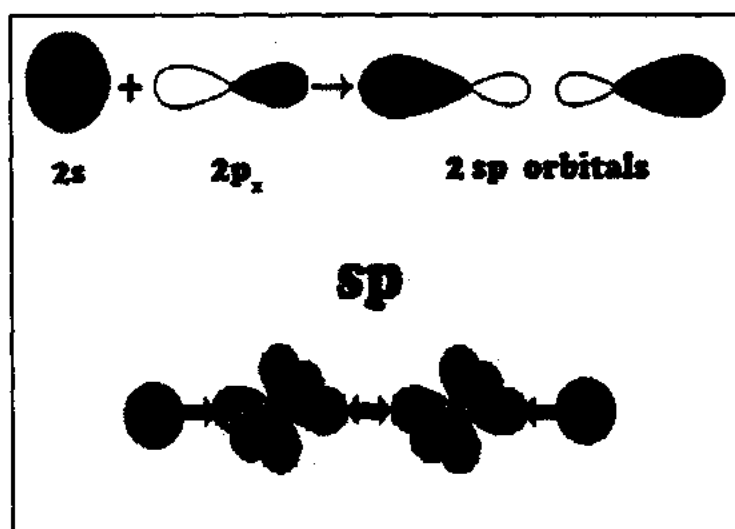


Figure 1-5: sp Hybridization [7]

2. **sp^2 or Trigonal Hybridization:** In sp^2 hybridization, one $2s$ and two $2p$ orbitals participate, consequent in the development of three sp^2 hybrid orbitals known as Trigonal Hybridization as shown in Fig.1-4.
3. **sp or Diagonal Hybridization:** In sp hybridization, one $2s$ and one $2p$ orbital participate in hybridization, subsequent in the development of two hybrid orbitals called as sp hybrid orbitals as shown in Fig.1-5.

The hybridized orbitals made strong (covalent) σ -bonds while the non-hybridized orbitals built weak π -bonds. The sigma-bonds are oriented so as to have highest possible angle between one another. As a result carbon can form linear chains, planar sheets or bulk material depending on the hybridization. The linear form of carbon is identified as carbyne, the planar

sheet as graphene and the bulk material as diamond. If there is no long range order but a mix of sp , sp^2 and sp^3 bonds, the structure is amorphous [6].

1.2.5 Carbon Allotropes

Diamond, graphite and amorphous carbon are well-known carbon allotropes since thousands of years. They reflect the versatility of carbon. Diamond is abrasive while graphite is a good lubricant and amorphous carbon exists in both phases (diamond and graphite like structure) depending on the degree of sp^3 hybridization.

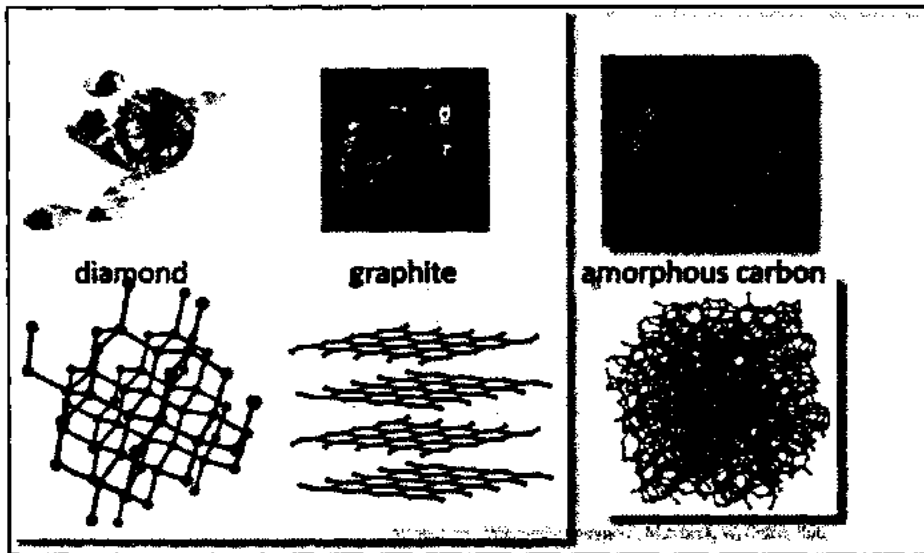


Figure 1-6: Different allotropic forms of carbon [8]

Graphite

Graphite is dynamically the best stable carbon structure under standard conditions. The structure of graphite had been elucidated by Debye, Scherer, Grimm, Otto, and Bernal in 1917. The basic unit of graphite is called graphene. It is characterized by a sequence of graphene layers that spread over a xy -plane. These layers are stacked along z -direction and bounded together with weak van-der Waals [9].

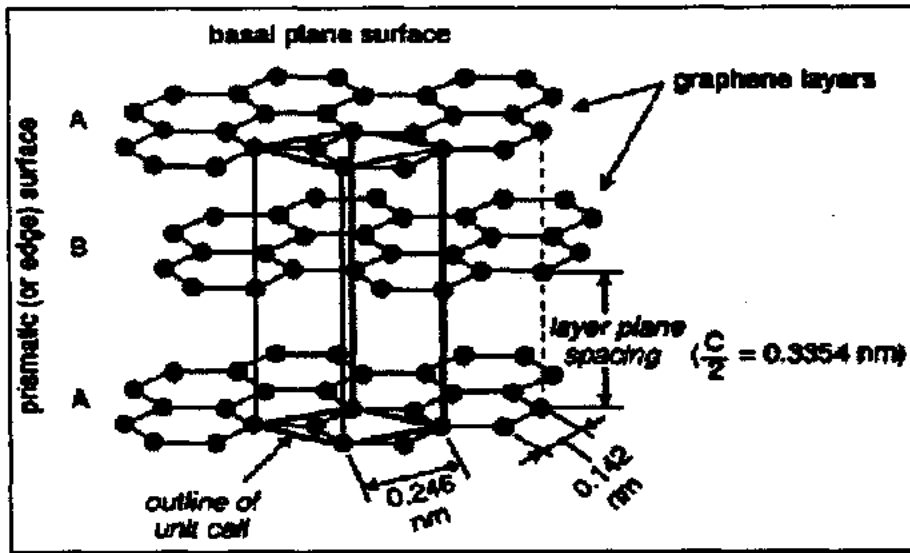


Figure 1-7: Three dimensional structure of graphite [10]

In each graphite layer, carbon atoms are organized in a hexagonal network with carbon to carbon distance is 0.142 nm, and the planes are separated by 0.335 nm as shown in Figure 1-7. Graphitic carbons fundamentally consist of sp^2 -hybridized carbon atoms which are organized in a planar “honeycomb-like” network. Vander Waals forces are responsible for a weak cohesion of the graphene layers generate layered graphite structure. Graphite powder has bulk density between 1.3 and 1.95 g/cm^3 and surface area 8.5 m^2/g . Graphite being the stiffest material has Young’s modulus around 1060 MPa, which is many times large than clay [8]. At room temperature, it has an excellent electrical conductivity of 104 S/cm. and the electricity is only passed within the plane of its layers. It is also a good conductor of heat and has a high melting temperature of 3500°C. Graphite is remarkably resistant to acid, extremely refractory, chemically inert, and has a low coefficient of friction. Its layered structure also provides a large anisotropy in the properties of graphite [11].

Graphite has two different modify cations, the hexagonal α -graphite, and the rhombohedral β -graphite. The rhombohedral β -graphite is relatively abundant in natural graphite and may be transformed into the thermodynamically more stable hexagonal form by the action of heat. The discrete graphene layers in the hexagonal structure are stacked according to an order ABAB with the atoms of a layer B being positioned above the centers of the hexagons in a layer A, and vice versa (Figure 1.8 a).

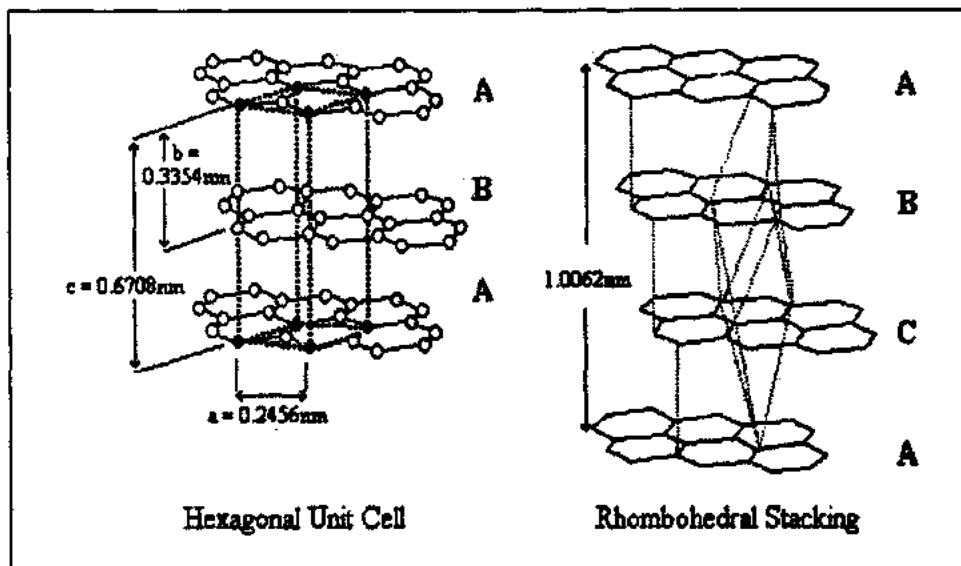


Figure 1-8: Arrangement of layers in hexagonal and rhombohedral graphite [12]

The third layer is congruent with the z-projection of the first one. The hexagonal unit cell consists of four carbon atoms, and the dimensions $(2.456 \times 2.456 \times 6.708) \text{ \AA}^3$. In rhombohedral graphite, the layers are stacked in an ABCABC sequence (Figure 1.8 b), bring about to a bigger unit cell $(2.456 \times 2.456 \times 10.062) \text{ \AA}^3$ that also contains four carbon atoms. Rhombohedral form is converted into α -form above $1025 \text{ }^\circ\text{C}$, while the reverse transformation may be attained by milling. The enthalpy of formation is about 0.06 kJ mol^{-1} higher for rhombohedral than for hexagonal graphite [13].

Diamond

The word diamond comes from the Greek word meaning unbreakable. In contrast to soft graphite, diamond is known hardest natural material. Diamond is an insulator with a wide band gap (5.5 eV). In diamond, each carbon atom has four immediate neighbors positioned at the corners of a tetrahedron. All carbon atoms are sp^3 - hybridized and the bond length uniformly is 154.45 pm. The crystal lattice of normal diamond is face-centered cubic (FCC) with a lattice constant of 356.68 pm and its unit cell has eight atoms.

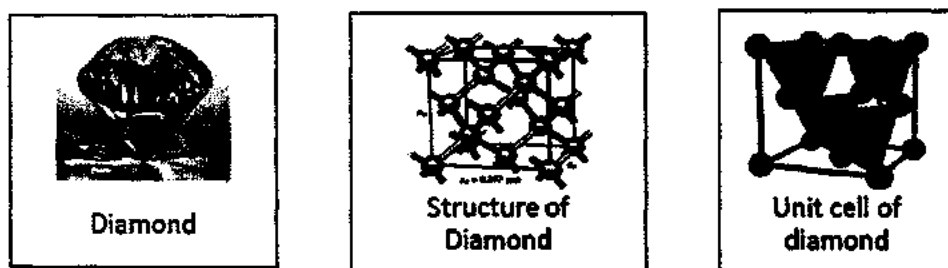


Figure 1-9: Diamond and its crystal structure [14]

Diamond also displays a great resistance to compression due to its tetrahedral structure. To measure the hardness of a crystal, Friederich Mohs developed a scale called Mohs, which grades compounds according to their ability to scratch one another. Diamond is known hardest material due to its highest value 10 on Mohs scale and has ability to scratch all other materials. Diamond is the best conductor of heat, conducting heat five times more than that of copper. Sound waves can pass through it, but not electricity. As diamond is a good insulator, its electrical resistance, chemical inertness and optical transmissivity are congruently remarkable. Additionally, diamond scatters light with refractive indices for red is 2.409 and for violet light are 2.465. Therefore, it works like a prism to dispersed visible spectrum (white light) into rainbow colors [15].

Table 1-2: Comparison between properties of graphite and diamond

Physical properties of graphite and diamond		
Properties	Graphite	Diamond
Color	Black with metallic luster	Colorless
Density @ 293 k (g/cm^3)	2.26	3.514
Refractive Index (at 546 nm)	2.15 \parallel ; 1.81 \perp	2.43
Specific resistance	$0.5 \times 10^{-4} \Omega \text{ cm}$ \parallel ; $0.2-0.1 \Omega \text{ cm}$ \perp	$10^{14}-10^{16} \Omega \text{ cm}$
Hardness (Mohs)	1 \parallel ; 4.5 \perp	10
Thermal Conductivity ($\text{W}\cdot\text{m}^{-1}\cdot\text{K}^{-1}$)	25-470	2500
Band gap (eV)	0	5.5
Electrical Conductivity (S cm^{-1})	4000, Conductor	10^{-13} , Insulator
Combustion Enthalpy ($\text{K J}\cdot\text{mol}^{-1}$)	393.5	295.4
Charge mobility ($\text{cm}^2\cdot\text{V}^{-1}\cdot\text{S}^{-1}$)	200,000	100,000
Mohs hardness scale	1-2	10

Amorphous carbon

Amorphous carbon (also called diamond-like carbon) does not have any crystalline structure. These materials are free, reactive and can be made stable by removing dangling- π bonds with hydrogen atom. Then these stable carbon materials are known as hydrogenated amorphous carbon. General amorphous carbons are symbolized by aC, hydrogenated amorphous carbons by aC:H or HAC and tetrahedral amorphous carbons by ta-C.

In mineralogy, soot, coal, carbide-derived carbon, and other impure forms of carbon which are neither diamond nor graphite, are all types of amorphous carbon. However, the

crystal structure of these materials is similar to polycrystalline materials, rather than truly amorphous [16].

True amorphous carbon has localized π electrons and nature of bonds, bond length and distances are all irregular as compared to any other allotrope of carbon. The concentration of dangling bond in these materials is very high; thus causing deviations in interatomic spacing of more than 5% along with observable change in bond angle.

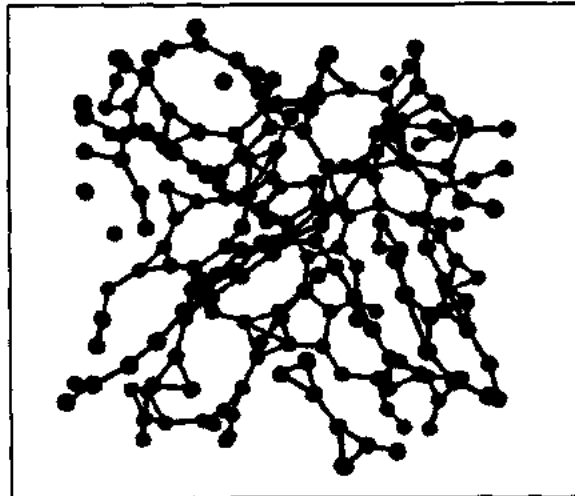


Figure 1-10: Ball & stick models of several amorphous carbon networks (red, blue and grey spheres are the sp^4 , sp^3 and sp^2 atoms, respectively) [17]

The most important technique for characterizing these carbon materials is to evaluate the ratio of sp^2 / sp^3 hybridized bonds. Graphite and Diamond have sp^2 and sp^3 hybridized bonds in their structure respectively. Therefore, materials that have high concentration in sp^3 hybridized bonds are called tetrahedral amorphous carbon (due to the tetrahedral shape made by sp^3 hybridized bonds) or diamond-like carbon (due to the resemblance of diamond's physical properties) [18].

1.2.6 Carbon-based Nanostructure Materials

Diamond, graphite and amorphous carbon are known carbon allotropes since thousands of years while its low dimensional allotropes form collectively called as carbon-based nanostructure materials. These materials synthesized and characterized at nano level have following three important forms:

- i. Fullerenes
- ii. Carbon Nanotubes
- iii. Graphene

In 1985 Richard Smalley, Harold Kroto and Robert Curl described the discovery of the buckminsterfullerene ("Bucky balls") [19], a discovery that awarded them the Nobel Prize in Chemistry in 1996. Through this discovery the science field of carbon based nanostructured materials was introduced. Fullerenes are categorized as zero dimensional (0D) lacking extension beyond a nanometer. Another type of Bucky balls (Fullerenes) in tubular form of diameter ranging from 1 to 10 nm known as carbon nanotube (CNT) was discovered in 1991. Multiwall nanotubes are designed in a carbon Arc Discharge observed by Sumio Iijima in 1991, and after two years, single-wall nanotubes are independently developed by Iijima and Donald Bethune at IBM [20]. Carbon nanotubes are known as 1D carbon materials. In 2004 Andre Geim and Kostya Novoselov at Manchester University succeeded to extract the structure 2D material graphene from bulk graphite with a simple technique using adhesive tape [21]. Their work on graphene led to award them the Nobel Prize in Physics in 2010.

1.2.7 Carbon Nanostructured Materials of Different Dimensionalities

Different methodologies are in practice to categorize carbon nanostructured materials. The proper grouping system is influenced by the field of application of the nanostructured materials [22, 23]. Carbon nanostructured materials are categorized into four classes on the basis of dimensionalities:

- i. Zero dimension structures (e.g., fullerenes, diamond clusters)
- ii. One-dimensional structures (e.g., carbon nanotubes)
- iii. Two-dimensional structures (e.g., graphene)
- iv. Three-dimensional structures (e.g., nanocrystalline diamond, graphite)

Technically, a graphene sheet can be considered as a basic building block for other carbon nanostructured materials. Wrapping sheet spherically forms 0D fullerenes, rolling into cylinders forms 1D Carbon nanotubes, and stacking layers into piles forms 3D graphite as shown in Fig. 1-11.

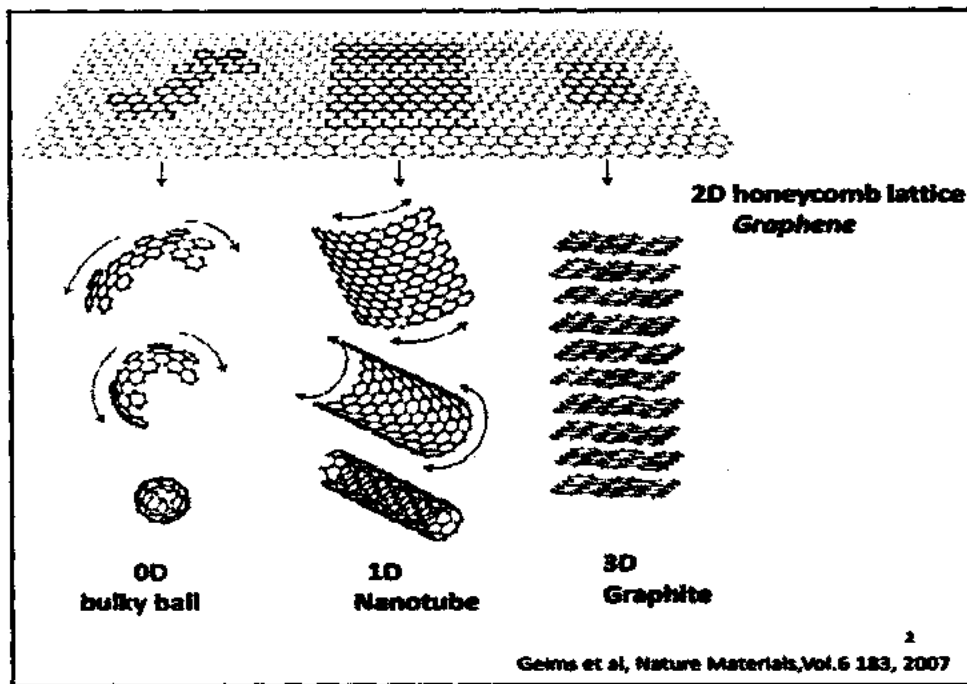


Figure 1-11: Graphene as a basic building block for all Graphitic forms [24]

Zero-Dimensional Carbon: Fullerenes

Materials having all spatial dimensions within the nanoscale (no dimensions, or 0-D, or less than 100 nm) are said zero-dimensional nanomaterials. Fullerenes have cage-like structure which can be considered as zero dimension (0D) carbon material. In 1985 Kroto et al. were able to produce C_{60} molecules, which have been named as Buckminsterfullerene, after Buckminster Fuller whose geodesic domes it resembles [25]. The discovery of C_{60} provided a strong signal for scientific community of the options of carbon materials and started gold rush in carbon research. Since discovery of C_{60} , many other fullerenes have been synthesized varying from the smallest fullerene C_{20} to C_{84} [26]. Also gigantic fullerenes consisting hundreds of atoms have been proposed [27], see Figure 1-12. All fullerenes are extremely strong cage structure which can bear high temperatures and pressures without breaking or changing the original shape.

Fullerenes have general formula C_{20+2n} and consist of hexagonal and pentagonal facets. In Fullerenes carbon atoms are sp^2 hybridized which are organized to the spherical-like configuration. The pentagonal facets try to bend it to spherical form while the hexagons tend to keep the surface flat. C_{60} (consists of isolated pentagonal facets) is the smallest possible fullerene. The isolated pentagonal facets will lower the energy of C_{60} and make it energetically more stable than smaller fullerenes. While C_{20} structurally minutest Fullerene is extremely

reactive, distinctly curved and it is very challenging to synthesize it without any surface contaminations [28, 29].

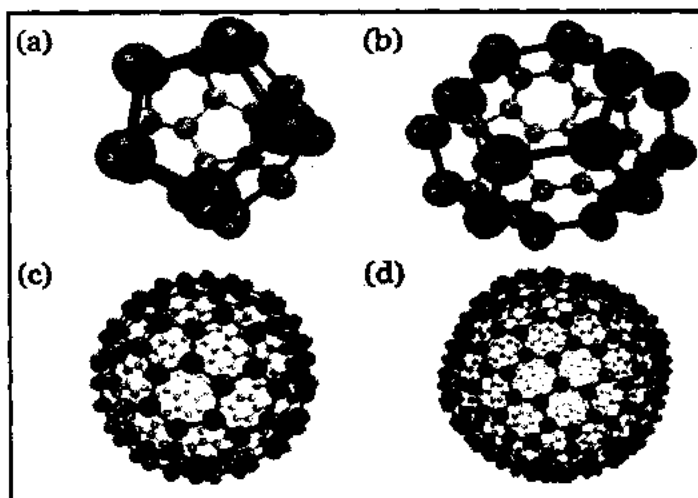


Figure 1-12: Different structures of Fullerenes (a) C_{20} (b) C_{40} (c) C_{240} and (d) C_{540} [30]

One-Dimensional Carbon: Nanotubes (CNTs)

One dimensional (1D) materials are those in which crystal size is negligible in two dimensional but not restricted in third dimensional. Carbon nanotubes are 1D cylindrical molecule and discovered experimentally by S. Iijima in 1991 with transmission electron microscopy, see Figure 1-13. The diameter of CNT is of nanometer size and its length can be as long as 18.5 cm. The scientific importance of CNTs is due to their exceptional electronic properties which are influenced by chirality. By modifying the diameter of carbon nanotubes and attaching different atoms on its surface, these can be either semiconducting or metallic in nature. Mechanical properties of the CNTs are also distinctive compared to other 1D nanostructure. In axial direction they are very strong but in radial direction nanotubes are quite soft. CNTs are very flexible and can withstand cross-sectional and twisting distortions and compression without fracture. These desirable mechanical properties make CNTs potential candidates for many applications relevant to everyday consumer [31].

Various techniques to synthesize CNTs have been developed. The most common methods are Chemical Vapor Deposition, Laser Ablation and Arc Discharge. The first CNTs were formed using Arc Discharge by Iijima in 1991. If one CNT is contained within another then it is categorized as a double-wall carbon nanotube (DWCNT) and if the CNT consists of more than two layers it is termed a multi-wall carbon nanotube (MWCNT).

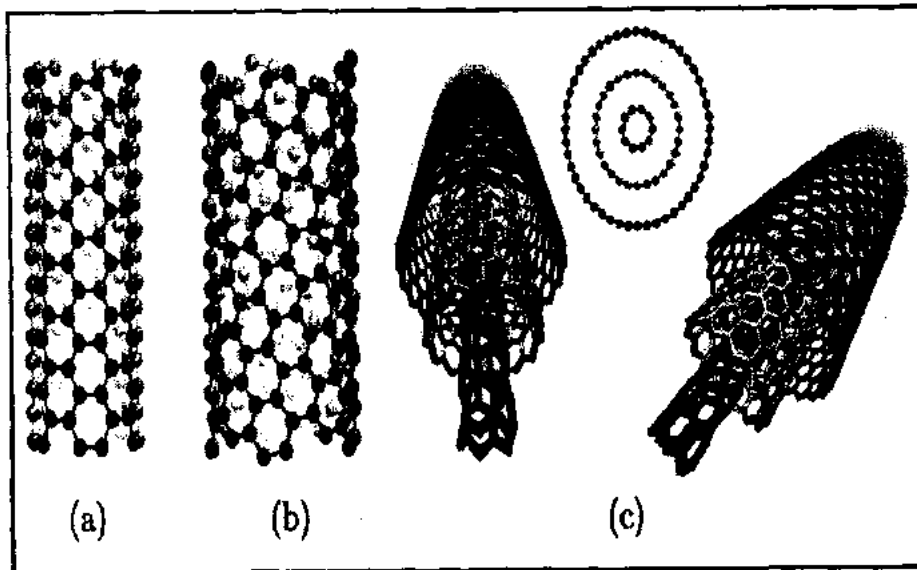


Figure 1-13: Different types of CNTs, Surface of (a) armchair (b) chiral CNTs, (c) Schematic presentation of Multi-Wall CNT [30]

Two-Dimensional Carbon: Graphene

Two-dimensional materials are those whose two dimensions are not confined to the nanoscale but are restricted in one dimension. For example, graphene is a 2D carbon material.

Three-Dimensional Carbon: Graphite

Three-dimensional materials are those whose no dimension is confined to the nanoscale. Diamond and graphite are the most well-known form of three-dimensional carbon material, which has been discussed in previous section (carbon allotropes).

1.3 Graphene

Graphene is a two-dimensional (2D) carbon material with thin sheet of carbon atoms that are organized in a hexagonal structure like honeycomb network. Graphene sheets with an interplanar spacing of 0.335 nm stack to form graphite and carbon to carbon bond distance is 0.142 nm. For many years it was understood that graphene does not exist in free state but is arranged to stacks forming graphite [32].

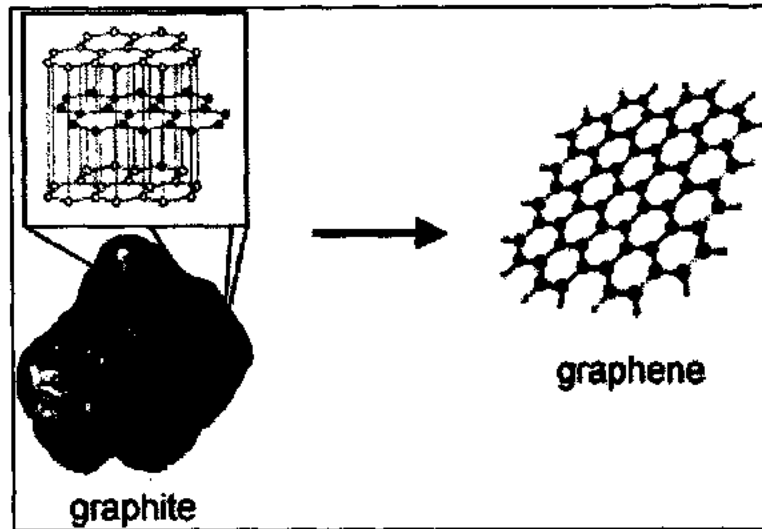


Figure 1-14: Isolation of graphene from graphite [33]

Though graphite had been used for centuries, individual graphene layers were isolated for the first time just recently by Novoselov et al. In each one of these sheets, carbon atoms occupy the vertices of hexagons in the honeycomb lattice. They form a very strong σ bond with the three adjacent atoms through sp^2 hybridization. The remaining $2p$ orbital is then available to form a π bond with adjacent atoms. The so formed extended π -electron network permits the flow of electrons in graphene and decides its optical and electrical properties [34]. One of the most significant achievements in 21st century is the discovery of graphene and its experimental observations. For this groundbreaking experiment, the Nobel Prize in Physics was given jointly to Konstantin Novoselov and Andre Geim in 2010.

1.3.1 Electronic Structure and Bonding of Graphene

Graphene is the atomically thin layer of carbon atoms in sp^2 arrangement. The angle between the sp^2 orbitals are 120° and carbon atoms binding only to other carbon atoms in this configuration will reduce in a honeycomb crystal lattice, infinitely wide but only one atom thick. With atoms forming only three bonds out of the available four, graphene is left with an out of plane delocalized π -bond network is shown in Figure 1-15. The primitive cell in reciprocal space, the Brillion zone in graphene is shown in Figure 1-16. The bonding and anti-bonding orbitals meet at Dirac points in the K- and K'-points of the Brillion zone forming Dirac cones with increasing energy gap towards the M- and Γ -points. Figure 1-17 illustrates the electronic band structure in the Brillion zone of graphene. Independent of the viewpoint the result is an exceptionally high electron mobility and correspondingly low resistivity [35].

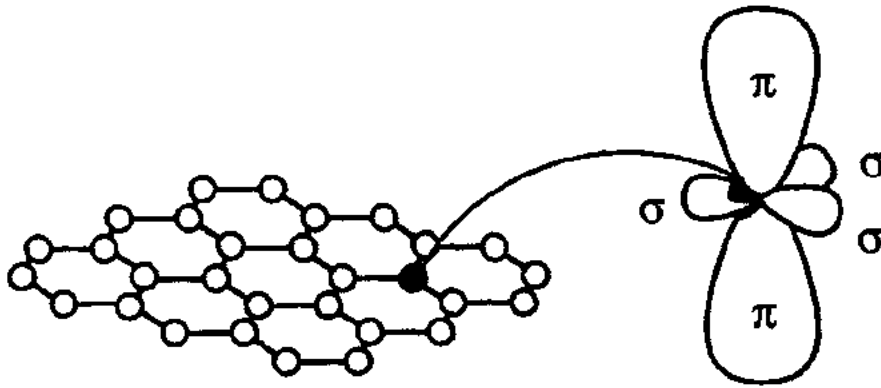


Figure 1-15: sp^2 hybridization in graphene [36]

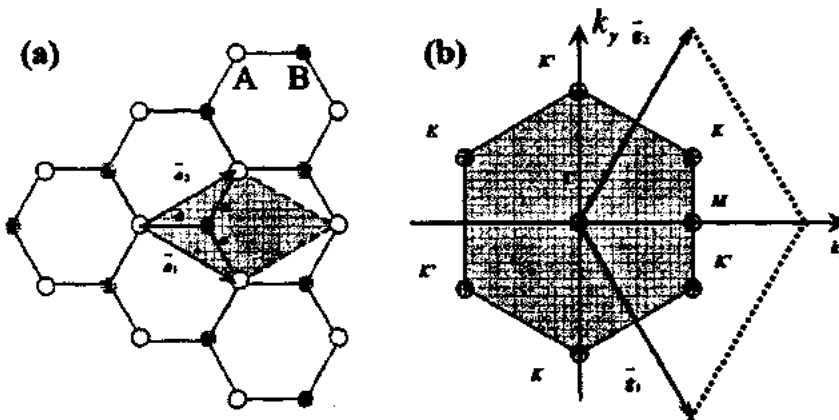


Figure 1-16: Graphene and its reciprocal lattice (a) Lattice structure of graphene, a_1 and a_2 are the lattice vectors. Shaded area shows graphene unit cell holds two carbon atoms A and B. (b) g_1 and g_2 are the reciprocal lattice vectors of graphene. The corresponding first Brillouin zone is depicted as the shaded hexagonal. The Dirac cones located at K and K' points [37].

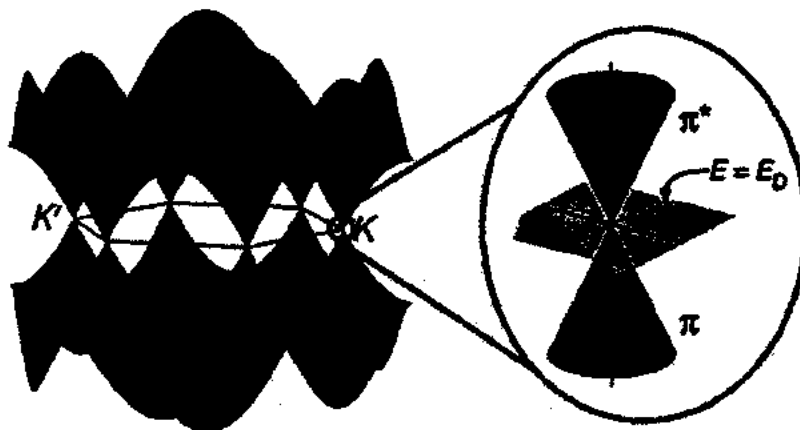


Figure 1-17: Schematic representation of band structure of graphene with two in-equivalent k- and k'-points, at the vertex of Brillouin Zone display no energy band gap between two sub lattices [38]

Isolated from any surroundings, graphene would have lower resistivity than silver. However, electron scattering due to phonon interaction from contact surfaces at room

temperature decreases the electron mobility and increases resistivity. Other extraordinary properties of graphene include a thermal conductivity exceeding that of diamond which is otherwise known as the best conductor of heat. According to Changgu Lee et al., graphene is to date the strongest material known to man with contravention strength 200 times greater than that of steel [39].

1.3.2 Why Graphene is Important?

- ▶ It has the capability of replacing silicon in the field of electronics for the next generation devices
- ▶ Its planar structure helps to develop electronic devices and has multiple electrical properties
- ▶ It measures one-atom in thickness, and can help to develop nano-scale devices
- ▶ Graphene is a good electric and thermal conductor and can be used to make computer parts and semiconductor circuits
- ▶ It also facilitates laboratory tests in physics that involve quantum mechanics and relativity

Table 1-3: Comparison between properties of graphene and carbon nanotubes

Properties	Graphene	Carbon nanotubes
Dimensions	2D	1D
Density @ 293 k (g/cm^3)	2.26	1.33
Thermal Conductivity ($\text{W}\cdot\text{m}^{-1}\cdot\text{K}^{-1}$)	5000	3000
Specific surface Area	2630	400
Electrical Conductivity (S cm^{-1})	10^6	5000
Fracture Strength (GPa)	124	45
Charge mobility ($\text{cm}^2\cdot\text{V}^{-1}\cdot\text{S}^{-1}$)	200,000	100,000

1.3.3 Single, Double and Multilayer Graphene

The electrical and electronic properties of graphene are influenced significantly by the number of layers (Geim and Novoselov, 2007). Normally the graphene community differentiates among mono-layer, double-layer, few-layer and multi-layer graphene. One sheet of graphene placed on top of another is known as bilayer layer graphene and when the number of layers is in the range 3–9 it is known as few-layer graphene. Multi-layer graphene is a structure consisting of more than 10 and less than 100 graphene layers and bulk graphite as

the number approach infinity. Stacked graphene can also form turbostratic carbon if the sheets are slightly shifted from the graphite (optimum) alignment [40, 41].

Single-layer Graphene

Single-layer graphene is consists of a honeycomb like structure of carbon atoms as depicted in fig. 1-18(a). Its unit cell (shaded area) contains two sublattices represented by A and B. All carbon atoms are bounded by sp^2 hybridization which make sigma bond with each other while delocalized pi electrons form pi bond. It has zero band gaps [42, 43].

Bilayer Graphene

Two layers of graphene bounded together in AB (Bernal) arrangement is called bilayer graphene [44] as displayed in figure 1-18(a). Graphene unit cell (shaded area) contains A and B layers. The distance between these two stacked layers is 0.334 nm and lie directly above or below each other [45].

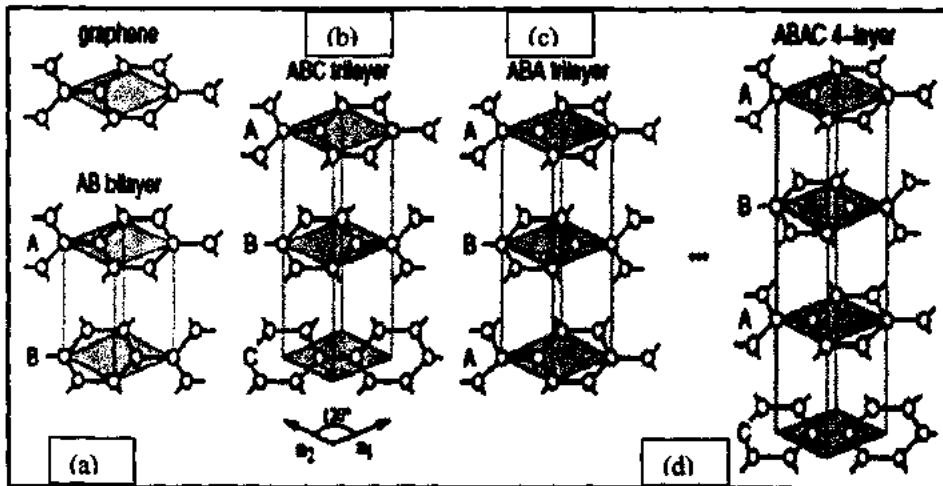


Figure 1-18: 2D primitive cells of Graphene with different stacking sequences [46]

Multilayer Graphene

A two dimensional material, (either as a substrate-bound coating or free-standing flake) contains 2-10 stacking structure of graphene layers is called multi-layer graphene [47].

A range of different stacking structures is possible in multilayer graphene due to weak Van der Waals forces among layers, giving different electronic properties [48]. The AB-stacking is recognized as the most stable arrangement of graphene layers. In this stacking arrangement, sublattice A on one honeycomb layer lies exactly below (or above) sublattice B on the other honeycomb layer as shown in figure 1-18(b). If graphene layers are stacked of more than 3 layers, then two arrangement of layers are possible as ABA (Bernal or hexagonal) [49] and ABC (rhombohedral) stacking [50] as displayed in figures 1-18(c) and 1-18(d),

respectively. In natural graphite, the ABA stacking arrangement is common and highly stable, while ABC takes some portion partly.

Stacking arrangement sensitively influences the electronic band structure of multilayer graphene. Multilayer graphene with ABA-stacking sequence, the spectrum comprises of superimposed linear (like monolayer graphene) and quadratic bands (like Bilayer graphene) [51], whereas the ABC multilayer graphene order has an absolutely dissimilar spectrum [52]. Optical measurement techniques are extensively implemented to calculate the electronic properties of layered graphene system, while Raman spectroscopy is implemented to evaluate the number of layers and stacking structure [53].

1.4 Graphene Nano-Platelets (GNPs): Our material of interest

Graphene is a mono-layer of carbon atoms arranged into a hexagonal lattice having 2D structure. It has highly applicable electronic properties that depend on the number of graphene layers. For a number of layers of about 2-5, they are called few layered graphene, graphene layers stacked 3-10 layers are known as multi-layer graphene, around 10-100 layers of graphene are known as Graphene Nanoplatelets (GNPs) [54, 55]. Graphite consists of hundreds to thousands of graphene layers. Graphene Nanoplatelets are structurally considered in between graphene and graphite; neither they are like single sheet of graphene, nor graphite. Thus on the basis of number of layers, graphene, GNPs and graphite can easily be differentiated. GNPs are inexpensive as compared to carbon nanotubes and single sheet of graphene. They have normally grain size in nano-meter thickness (stacking height) with micro sized diameter, giving them high aspect ratio (thickness/diameter).

1.4.1 Why Graphene Nanoplatelets are Important?

Graphene Nanoplatelets (GNPs) are effectively used in providing barrier properties due to their unique size and platelet morphology, whereas their pure graphitic configuration proves them outstanding thermal and electrical conductors. GNPs can also be used to enhance mechanical properties like surface hardness, strength, and stiffness of the matrix material [56]

During the last several years, graphene research has developed at a very rapid pace. However at present, high cost and low yield of graphene have been hampering its research and application. In recently years, GNPs which are comprised with several stacked graphene sheets have emerged to offer more possibilities for expanding the on-going development of graphene. Compared with graphene, GNPs have much lower production cost and better

stability. GNPs and their composites exhibit good mechanical and electrical properties [57–59] which enable them for potential applications such as in protein detection [60, 61] photomechanical actuation [62] and in thermo conductive materials [63].

1.42 Characteristics of Graphene Nanoplatelets (GNPs)

- ▶ GNPs have very high Young's modulus ($\sim 1,000$ GPa) and high strength (~ 130 GPa estimated).
- ▶ In composite materials, GNPs can offer an efficient moisture barrier
- ▶ GNPs have excellent electrical Conductivity along the plane ($\sim 20,000$ S/cm).
- ▶ They have density 2.26g/cm^3 which is four times lower than copper
- ▶ GNPs have thermal Conductivity equal to $5,300\text{Wm}^{-1}\text{K}^{-1}$ which is five times more than that of copper.
- ▶ GNPs have high range of specific surface area from 20 to $1500\text{m}^2/\text{g}$ depending on their methods of preparation
- ▶ They have density (2.26g/cm^3) much lower than steel but have strength 50 times stronger than steel
- ▶ They have very good opposition to gas infiltration.
- ▶ They can be dispersed in common solvents and many polymers
- ▶ Due to their nano-scaled size, they can be used as filler for composites.
- ▶ GNPs in nano-composites have high loading up to 75 wt.% [64]

1.43 Applications of Graphene Nanoplatelets

Graphene Nanoplatelets (GNPs) are an excellent additive to plastics of all types, and can be an energetic constituent in coatings or inks as well as compatible with almost all polymers. Due to non-oxidizing nature and a pristine graphitic surface of sp^2 carbon molecules, GNPs are exclusively useful in high thermal or electrical conductivity locations [65].

- ▶ GNPs are used in Ultra capacitor electrodes
- ▶ They are used as anode materials for lithium-ion batteries
- ▶ Graphene Nanoplatelets can be used as Conductive additive for battery electrodes and for making lightweight composites
- ▶ GNPs are used in electrically conductive inks
- ▶ Flexible touch displays, solar cells and photovoltaic can be made by GNPs
- ▶ They are used in making thermally conductive films and coatings for EMI shielding

- ▶ GNPs are used as substrate for chemical and biochemical sensors
- ▶ They have tremendous application as barrier material for packaging
- ▶ GNPs can be used as additive for super-strong concrete and metal-matrix composites
- ▶ Due to their absorptive behaviors (great chemical bonding to a wide range of resins), GNPs are used in areas of energy production for a cleaner environment
- ▶ GNPs are also used as a filter, for purifying harmful organic and in-organic materials (heavy metals and radionuclides) from wastewater and ground water.

Conclusively, in future GNPs will be the part of electronic circuits due to their nano-scaled size, lower resistance, lower voltage and faster in current conduction.

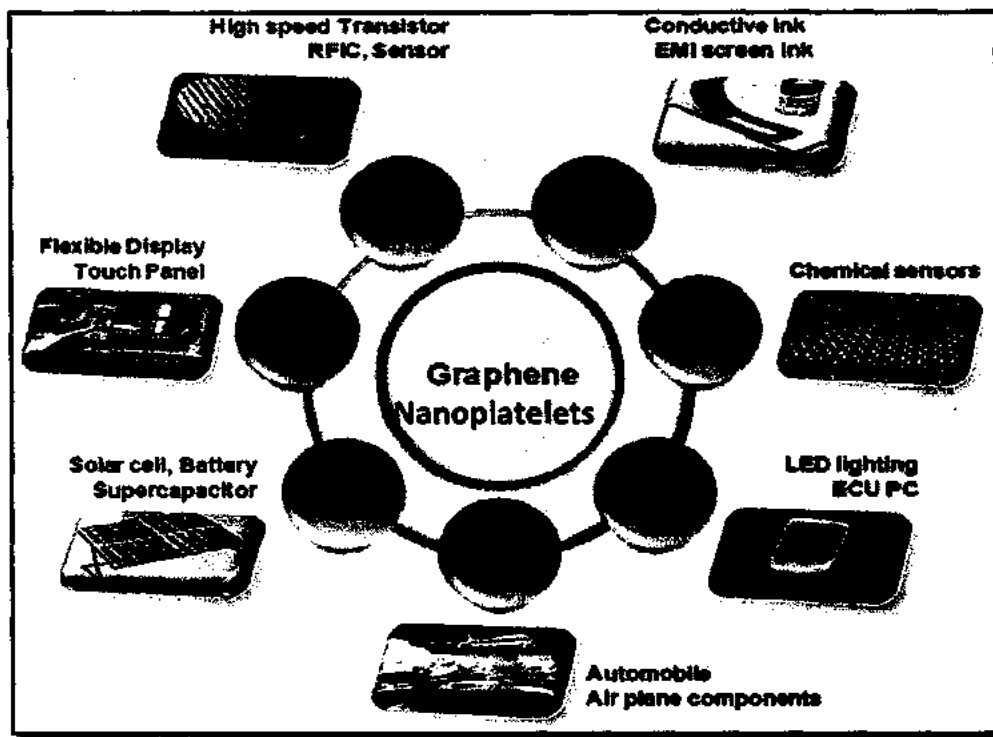


Figure 1-19: Overview of Applications of Graphene Nanoplatelets (GNPs) [66]

1.5 Heat Treatment

Heat treatment states the heating and cooling processes required to modify the characteristics of ceramic materials, alloys plastic and metals. Heat treatment means when a material has been heated beyond a certain temperature, it experiences a structural modification on cooling to room temperature.

The objective of heat treatment is to attain any one or more aims cited as follows:

- ▶ To eliminate strain hardening of a cold worked metal and to elevate its ductility

- ▶ To release inner stresses established during cold/hot-working treatments
- ▶ To enhance the cutting ability and to improve grain structure after hot working a metal
- ▶ To increase magnetization property of steels

1.5.1 Thermal Annealing

Thermal annealing or simply annealing is a type of heat treatment in which a material attains a structure near to the equilibrium one after heating to certain temperature. In thermal annealing, a material is placed in a high temperature environment for a long time period and then gradually cooled.

Annealing is performed to relieve stresses, enhance softness, ductility and create a particular microstructure. In thermal annealing, temperature of heating relies on the configuration of material and the specific type of the process.

The process of thermal annealing comprises of three phases:

- (i) Heating the material to the required temperature
- (ii) Holding the material at that temperature for a specific time
- (iii) Cooling slowly, generally to room temperature

In thermal annealing processes, time is a key factor. Temperature gradients exist between the interior and outside parts of the material during annealing process. The magnitude of temperature gradients basically depends on geometry and the size of the heating material. The temperature gradients are typically 30-200°C/h. If the magnitude of temperature gradients is too great, then stresses may be produced inside the material that may give an increase in folding and cracking.

1.5.2 Recovery, Recrystallization and Grain Growth

When a material (normally metal) is plastically deformed at low temperatures (~ 25 °C) a change in microstructural and property occurs. These include:

- ▶ A variation in grain size and shape
- ▶ Strain hardening
- ▶ An enhancement in dislocation density

The changes in structure and property of the material can revert back to the pre-cold worked states by proper thermal annealing, i.e. heat treatment. Such reclamation of properties is the result of two dissimilar processes i.e., recovery and recrystallization that happen at high temperatures. Recovery occurs at comparatively low temperatures and recrystallization at higher temperatures.

Recovery

This term means that all alterations only involve in the fine structure and it does not alter the shape and size of grains. In the course of this process, some of the stored inner strain energy is released as a result of displacement motion and increased atomic dispersion at high temperature. Also, thermal and electrical conductivities are recuperated to their pre-cold-worked states.

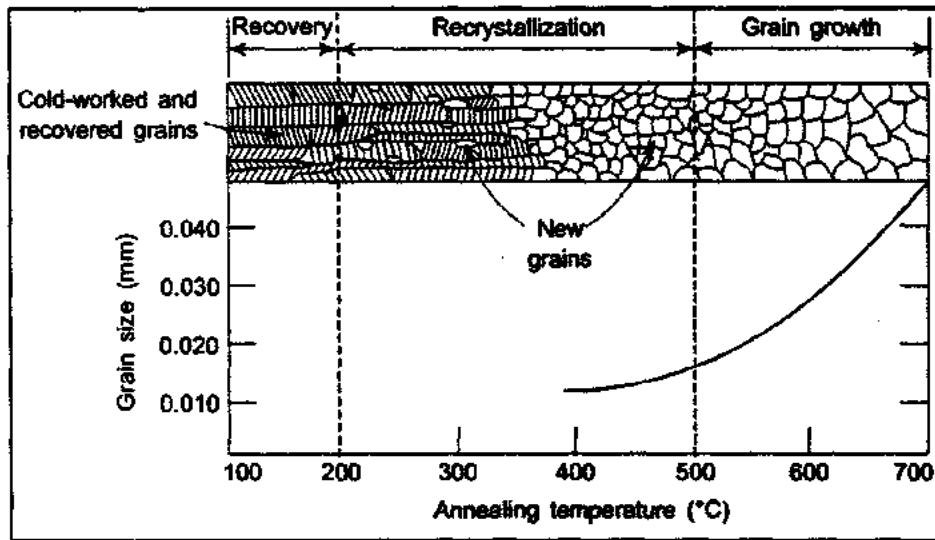


Figure 1-20: Grain size versus annealing temperature is displayed. Grain structure during Recovery, Recrystallization and Grain Growth phases are presented [67]

Recrystallization

It is a process in which nucleation and growth of new grains occur with minimal structural defects. As a result of Recrystallization, completely new most often equiaxed crystals are created. The variation in inner energy between the strained and unstrained material is the chief dynamic force to create this new grain structure. The new grains generate at the cost of small nuclei and grow until they totally devour the parent material. This process comprises of short-range diffusion and may be used to improve the grain structure.

Grain Growth

In the course of recrystallization process, the nucleation of new grains happens in the areas of the maximum dislocation density, generally at the boundaries of distorted grains. The larger the plastic deformation, the more recrystallization centers develop in a metal. These centers are basically submicroscopic zones with the minimum amount of point and linear defects in the structure. These regions grow due to reorganization and limited demolition of dislocations. With the passage of time, centers of new grains increase in size as a result of transport of atoms from the distorted portions to a more perfect lattice [67].

CHAPTER NO.2

2 MATERIAL AND METHODS

2.1 Sample Preparation

Commercially available purified Graphene Nanoplatelets (KNG-150, Xiamen Knano Graphene Technology Co., Ltd, China) powder with carbon content of 99.99% were used to prepare pellets using Desk-top Powder Presser (Model YLJ-24T).

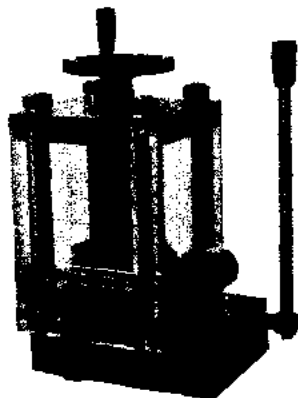


Figure 2-1: Desk-top Powder Presser (Model YLJ-24T) [68]

2.1.1 Procedure

Graphene Nanoplatelets (GNPs) in the form of powder are put on the center of the working stage. The spinning screw is turned down toward the sample. The oil release valve was opened. Then swang the rocker 3 to 4 times forth and back and tighten the oil release valve. The pressure was increase up to 20 MPa. This pressure was kept for 15 minutes before opening the oil release valve. GNPs were pressed in to pellets of diameter 13 mm and of thickness 3 mm. These pellets had almost same weight, diameter and thickness and pressed for same duration.

2.2 Vacuum Annealing of Prepared Samples

The simple annealing experiment was performed in the quartz tube reactor described in Figure 2-2. Before starting the annealing process, the furnace was evacuated by vacuum pump to create vacuum in the tube. The five out of six pressed pellets of GNPs were introduced into the furnace and thermally annealed at 300, 500, 700 900 and 1100 °C for one hour under vacuum condition. The heating rate was 5 °C per minute. The annealed pellets were named as G300, G500, G700, G900 and G1100 heated at temperatures 300, 500, 700,

900 and 1100 °C respectively and one un-treated sample named as Grt (rt means room temp.). After thermal annealing, the annealed samples were cooled down to room temperature and drawn from furnace for further analysis.

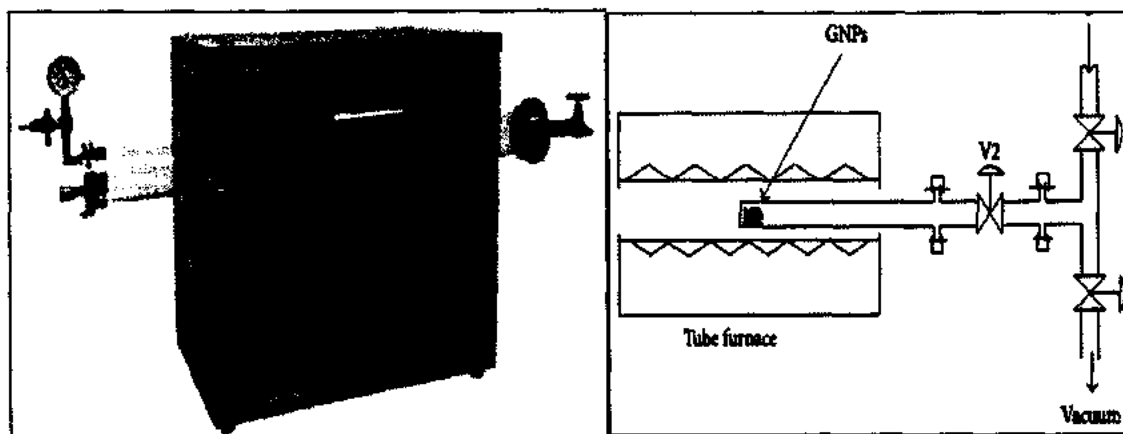


Figure 2-2: High Temperature Vacuum Tube Furnace with block diagram for annealing of GNPs [69]

CHAPTER NO.3

3 CHARACTERIZATION TECHNIQUES

To characterize Graphene Nanoplatelets structure and their morphology, different techniques like X-ray Diffraction, Field Emission Electron Microscopy and Raman spectroscopy have been used. In characterization, we determine the physical properties and morphology of a nano structured material.

To characterize nanostructures materials different techniques has been used such as:

- ▶ X-Ray Diffraction (XRD)
- ▶ Field Emission Scanning Electron Microscopy (FE-SEM)
- ▶ Raman Spectroscopy
- ▶ LCR Meter

Among these, XRD is the most commonly used technique for quantitative analysis. A brief description of XRD technique is given below.

3.1 X-Ray Diffraction (XRD)

XRD stands for X-Ray Diffraction. In 1895 a German Physicist Sir William Rontgen discovered X-ray during investigation of Crooke's tube experiment. It is the best way to know the given material whether it is crystalline, polycrystalline or amorphous and also assistances us to calculate the crystal structure, size and shape. Roentgen revealed that when a beam of electrons strike with any target material, it emits radiations. These radiations were named as X-rays.

3.1.1 Working

X-ray diffractometers contain three main parts: an X-ray tube (source of radiation), a sample holder, and a radiation detector. X-ray tube contains a filament (cathode) which emits electrons on heating. These electrons are accelerated towards anode (Tungsten) by high voltage.

Characteristic X-rays are generated, when these high energy electrons hit inner shell electrons of the target (Tungsten) to eject them. The wavelengths of the emitted X-rays depend on of the type of target material (Copper, Chromium, Ferric and Molybdenum). X-rays of mono wavelength required for crystal diffraction, are produced using filter.

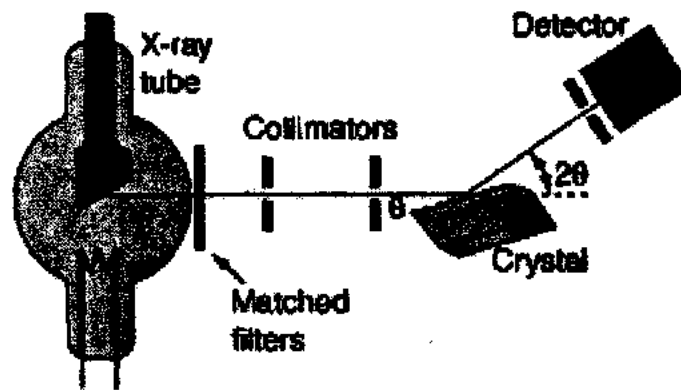


Figure 3-1: Main parts of X-ray Diffractometer [70]

For diffraction of a single-crystal, Cu is commonly used element for target material, with Copper K_{α} radiation of wavelength 1.5418\AA . These parallel and in line X-rays are focused onto the material. The intense reflected X-rays are recorded (in the form of peak) due to constructive interference on rotating the material and detector. Constructive interference only occurs if conditions satisfy Bragg's Law. However, destructive interference will occur if this condition is not satisfied and no peak will be seen. The reflected X-rays are processed and convert them to a count rate which can be seen on output devices such as computer monitor or a printer [70].

3.1.2 Bragg's Law

Bragg's law was discovered by Physicist Sir William Lawrence Bragg in 1912. He and his father (William Henry Bragg) awarded jointly Nobel Prize in 1915. According to this law, when a parallel and in line beam of X-rays having specific wavelength are incident on the atoms of a crystal with a certain incident angle θ , they are reflected with same angle θ from the crystal planes producing diffraction in the crystal lattice. When the path difference d of two incident waves is an integral multiple of the wavelength of X-rays, then a constructive interference will occur otherwise a destructive interference will occur when this condition is not satisfy. This law can be written in mathematical form as

$$n \lambda = 2d \sin \theta \text{ ----- (1)}$$

Where, λ is the wavelength of X-rays, d is the inter planer distance, θ is the incident angle and n (an integer) is the order of reflection [71].

XRD diffraction profile is plotted by taking the intensity of the diffracted X-rays along Y-axis and measured diffraction angle 2θ along X-axis. This diffraction profile is used to find the crystal structure, phases and size [72].

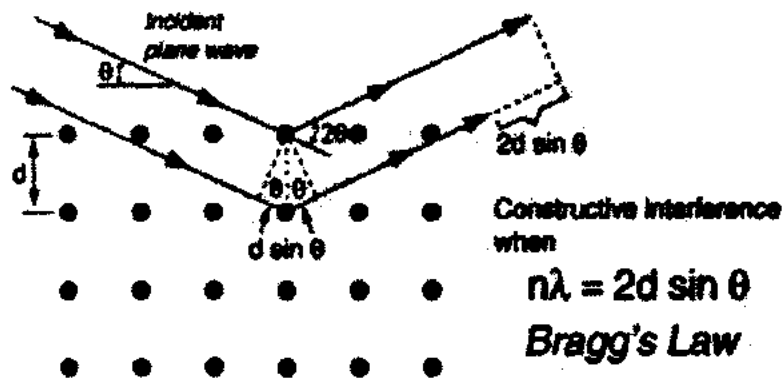


Figure 3-2: Schematic diagram of Bragg's Law [71]

The crystallite size, can be estimated using Scherer's

$$L = k \lambda / \beta \cos \theta \text{ ----- (2)}$$

Where β is the full width at half maximum (FWHM), K is the constant of proportionality (the Scherer constant) which depends on the shape of the crystal. K actually varies from 0.62 to 2.08. L is the size of the crystallites [73-75].

3.2 Microscopic Studies

Electron Microscopy is that particular field of science in which an electron microscope is used as an instrument which generates an image of a material with the help of electrons beam [76, 77]. A vacuum is created in Electron Microscopy (EM) and with the help of electromagnetic lenses, beam of electron is focused and finally a magnified image is obtained. To generate image, EM uses electrons of very smaller wavelength ($\lambda = 0.005 \text{ nm}$) in comparison with visible light of wavelengths ($\lambda = 400\text{-}700 \text{ nm}$) [78].

Electron microscopy has two main types:

1. The scanning electron microscope (SEM)
2. The transmission electron microscope (TEM)

Though SEM and TEM were developed within the same decade, they vary largely in their applications and uses. Briefly, in SEM, images are created by secondary electrons which are 3D image in nature, while the TEM projects electrons through a very thin piece of the sample and generate a 2D image [79].

3.2.1 Scanning Electron Microscopy

SEM is commonly used to characterize nanostructures, in particular to estimate their morphology (width) and not able to measure nano-sized powders. The working principle of a

SEM comprises an electron source (thermal field emission) that generates an electron beam, which is focused and deflected (raster-scanned) by a system of electromagnetic lenses over the sample surface, as schematically represented in figure 3.3a. Samples must be (partially) electrically conductive in order to avoid charging effects. The point at which the beam of primary electron strikes, secondary electrons (SE), backscattered electrons, X-rays and light are generated. The SE, having energy below 50 eV, are emerging directly from the uppermost nanometers of the sample. On a sloped surface more electrons are produced. The secondary electrons are collected by an in-lens SE detector. The beam is scanned above the surface and the position dependent intensity of SE is used for topographic imaging. The whole SEM chamber must be under vacuum, since otherwise the electrons would be dispersed by air molecules. A working distance (the distance between the sample and the final lens) of 1.5-5 mm and an electron acceleration voltage of 3-15 kV were adjusted, producing a maximum resolution of 1 nm. SEM was done after all other characterization techniques, due to the irreversible effect of beam of electron on the imaged material [80, 81].

77/5200

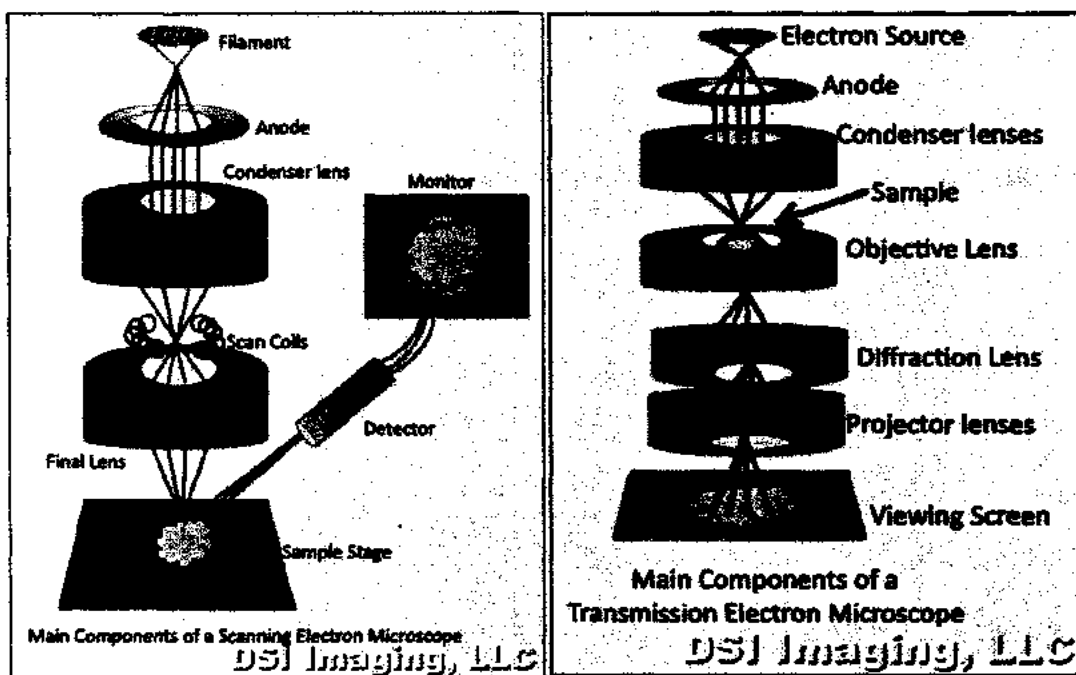


Figure 3-3: Schematic representation of SEM and TEM, showing their main components [78]

3.2.2 Energy Dispersive X-Ray Spectroscopy (EDS or EDX)

EDX is a chemical microanalysis method used in combination with SEM. The EDX system identifies X-rays radiation released from the material when a beam of SEM electrons hit the material electrons to identify composition of the element of the examined material.

Principle of EDX

When beam of SEM electrons is hit on the sample under observation, electrons are released from the surface atoms of the sample creating vacancies. The electrons from a higher energy state fill those vacancies, and an X-ray is released of energy equal to energy variation between the two electronic states. This X-ray energy is specific to the element from which it was radiated.

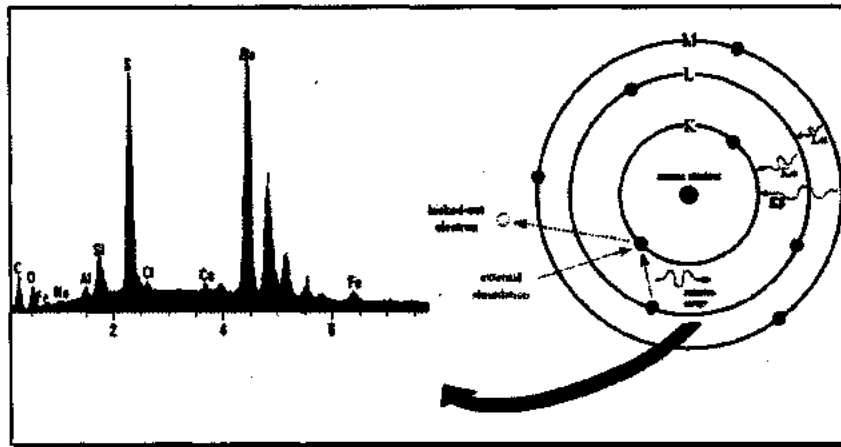


Figure 3-4: EDX basic principle with EDX spectrum [82]

Working of EDX

Typically Si (Li) detector is used to detect X-rays emitted from the sample. When an incident X-ray hits the detector, it generates a current pulse corresponding to the X-ray energy as shown in Fig.3-5.

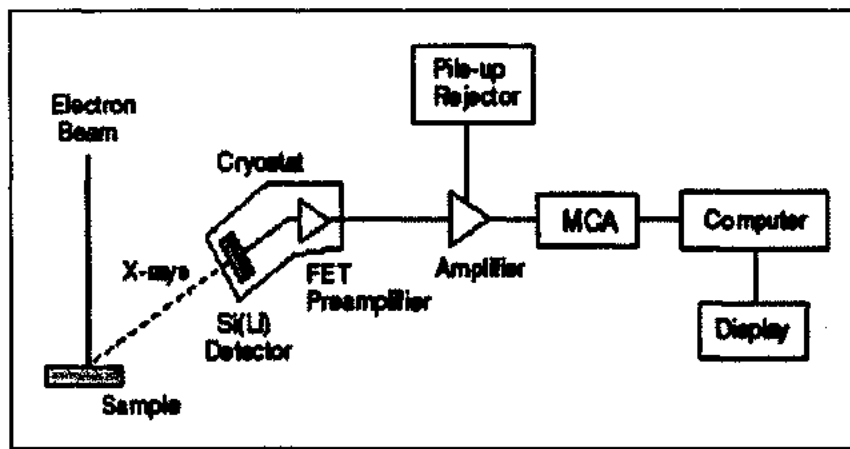


Figure 3-5: Schematic representation of an energy-dispersive spectrometer [82]

This current pulse is changed in to voltage signal using preamplifier and then sent to a multi-channel analyzer where these signals are separated and further sent to computer for display. To find the composition of elements of a material, x-ray energy spectrum versus counts is calculated as shown in Fig.3-4.

3.2.3 Transmission Electron Microscopy

In order to reach atomic resolution of GNPs, TEM was used at room temperature. If a sample is thin enough, electrons can be transmitted through the sample (direct and scattered). The increase in resolution of TEM compared to SEM has two origins. First higher electron energy corresponds to a shorter de Broglie wavelength, and secondly the thin sample provides a smaller interaction volume. In a TEM, electrons from an electron source are made into a parallel beam by a (electromagnetic) condenser lens (figure 3.3b). This beam passes through the sample and is then focused by an objective lens onto a Charge Coupled Device (CCD) with a scintillator material that converts incident electrons to light, or directly onto an electron detector. Spherical and chromatic aberration correctors enhance the resolution. The image information in high-resolution TEM depends on phase-contrast (one kind of operation mode of TEM). In phase-contrast imaging, interference of the scattered electrons leads to an image with atomic resolution. It was operated at a pressure below 10^{-7} mbar and voltage of 80 kV in order to reduce the radiation damage of the GNPs by electron bombardment [84].

3.3 Raman Spectroscopy

A further analysis step in the detection and investigation of Graphene Nanoplatelets is Raman Spectroscopy. Raman spectra for single, double, and multi layers reveal variations in the electron bands and permit clear and non-destructive identification of graphene layers [85]. Defects in the GNPs can also be identified and analyzed by this method.

3.3.1 What is Raman Effect?

The Raman Effect insisrences on inelastic scattering of monochromatic light released from a laser source. It indicates that in monochromatic light, the frequency of photons alters when it interacts with atoms of the sample. The sample absorbs photons of the laser light and then reemits photons. The frequency of the reemitted photons is increased or decreased with respect to the original monochromatic frequency. This is called the Raman Effect. These shifts in frequencies provide information about rotational and vibrational changes in the molecules. Due to this Raman Effect, molecular distortions take place in the presence of an electric field E.

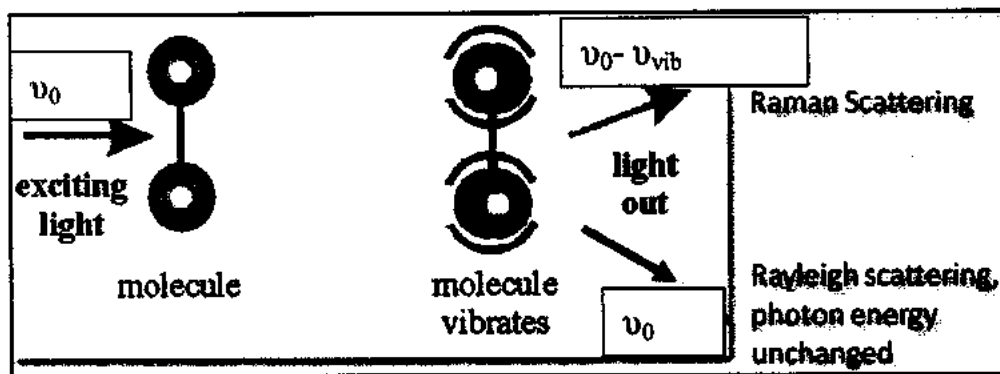


Figure 3-6: Block diagram of Raman and Rayleigh scattering [86]

Basically, a laser beam can be recognized as an oscillating electromagnetic wave having electrical field vector E . When monochromatic laser light with frequency ν_0 interacts with the molecule it produces an electric dipole moment $P = \alpha E$ where α is called molecular polarizability and P is dipole moment which is responsible to deforms molecules. These molecules start vibrating with a certain frequency ν_{vib} due to periodical deformation. Such oscillating dipoles emitted light of two different frequencies:

1. Rayleigh Elastic scattering
2. Raman in-elastic scattering
 - 2.1. Raman Stokes frequency
 - 2.2. Raman Anti-Stokes frequency

3.3.2 Elastic Rayleigh Scattering

This type of scattering has no Raman-active modes and the molecule absorbs an incident photon of light with frequency ν_0 . After absorbing photon, the molecule goes in to excited state and then returns back to the same vibrational state and radiates light with the equal frequency ν_0 as shown in Fig.3-6. This phenomenon is called elastic Rayleigh scattering

3.3.3 Raman in-elastic Scattering

3.3.3.1 Raman Stokes frequency

It is a type of inelastic scattering, in which an incident photon of light with frequency ν_0 is absorbed by a Raman-active molecule in its basic vibrational state. Part of the photon's energy is consumed to transfer the molecule to the Raman-active mode with frequency ν_{vib} and as a result the frequency of reemitted light is decreased to $\nu_0 - \nu_{vib}$. This decreased frequency is called Stokes frequency, as shown in Fig.3-6.

3.3.3.2 Raman Anti-Stokes frequency

It is also a type of inelastic scattering in which an incident photon of light with frequency ν_0 is absorbed by a Raman-active molecule, which is already in an excited vibrational state at the time of interaction. Part of the energy of the excited Raman active mode is absorbed; the molecule goes to a lower vibrational state and as a result the frequency of reemitted photon is increased to $\nu_0 + \nu_{\text{vib}}$. This increased frequency is called Anti-Stokes frequency [87].

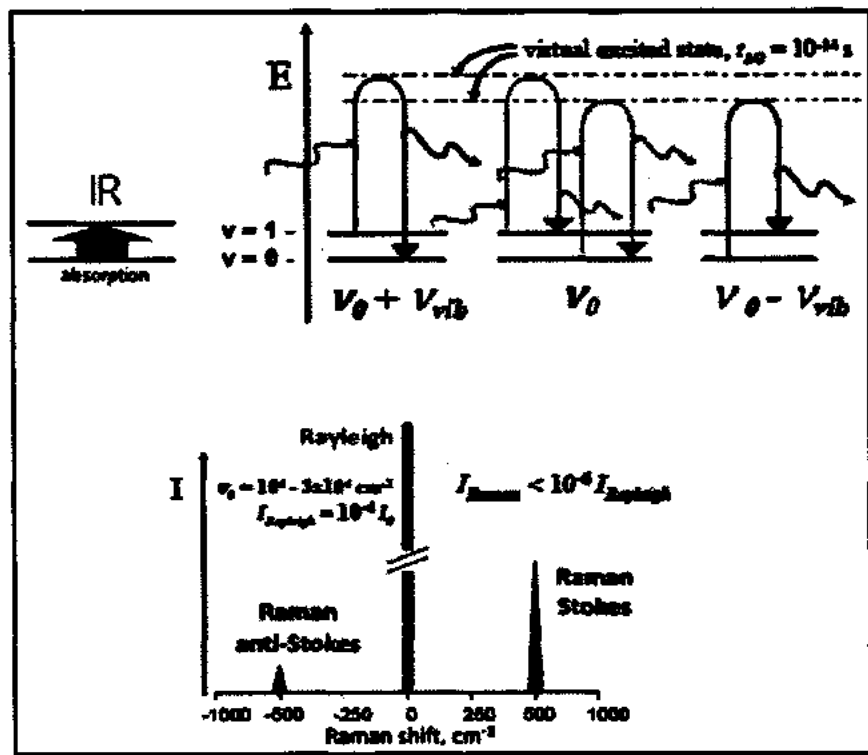


Figure 3-7: Raman Effect (Top) and (b) Raman spectrum (Bottom) [88]

A sketch of the Raman Effect and a typical Raman spectrum is shown in Fig.3-7.

From Fig.3-7 (bottom) it is clear that stokes and anti-stokes peak appear at symmetric positions of either side of 0 cm^{-1} . Normally stokes bands are stronger than anti-stokes, depending on the sample temperature and on the energy spacing of the vibrational levels (anti-stokes band should not appear at 0K).

In spontaneous Raman, almost 99.999% of all photons of incident light experience elastic Rayleigh scattering. This form of signature is impracticable for applied determinations of molecular characterization. Merely 0.001% of photons of incident light generates inelastic Raman spectrum with increased frequencies $\nu_0 + \nu_{\text{vib}}$ [87].

Raman spectroscopy is a very important analysis technique in the field of carbon research and has historically presented a significant role in the structural characterization of

graphitic materials [94]. In fact, this spectroscopy technique allows distinguishing clearly between single and multilayer graphene [89]. Fig 3-8 shows a Raman spectrum of monolayer graphene with respect to Raman spectrum of multilayer graphite.

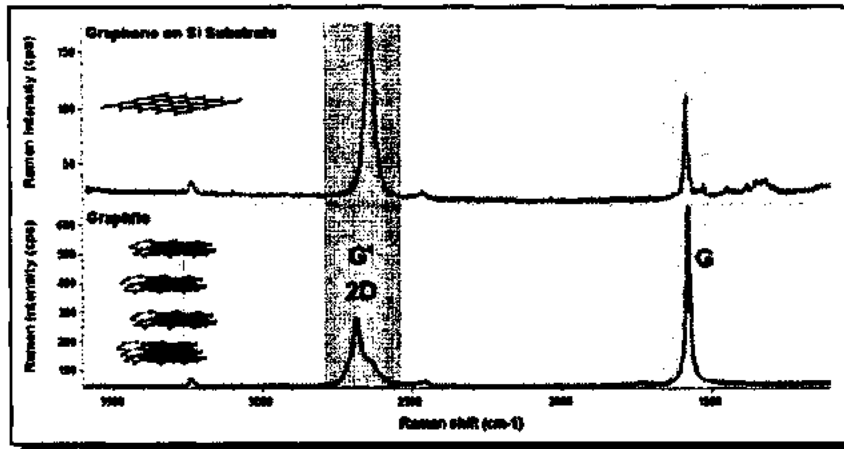


Figure 3-8: Raman spectra of (a) Graphene (top) and Graphite (bottom) [90]

Graphene has two important peaks: a first peak at 1580 cm^{-1} called the G peak, and a second peak at 2700 cm^{-1} named 2D peak. In monolayer graphene, the shape of the 2D peak is sharp, thin and centered at 2700 cm^{-1} . This peak broadens in thicker sheets, is the resulting envelop of four sub-peaks as shown in Fig. 3-9 [91].

A suitable tool to study the formation of defects in mono- or multilayer graphene is Raman spectroscopy. This is due to a so-called “defect peak” D present in the graphite and graphene spectra. The D peak intensity increases as the amount of defects increases.

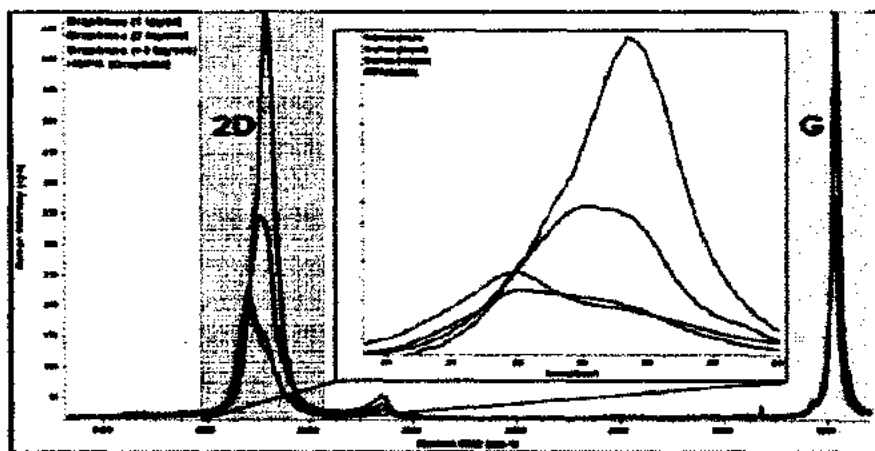


Figure 3-9: Comparison of Raman spectra of HOPG graphite, mono, bi- and tri-layers graphene [90]

Raman spectroscopy has been used to examine carbon-based materials due to the explicit response to any modification in carbon hybridization state, as well as to investigate defects. To study defects, graphene is a perfect material due to its two dimensional structure.

It is easy to move, add or remove (defects) carbon atoms in graphene honeycomb network as compared to graphite or carbon nanotubes. Therefore, graphene being a perfect material can be used to study the nature of defects by Raman spectrum. Moreover, information about the impurity of the sample can be obtained from the I_D/I_G intensity ratio [92, 93] (see Fig. 3-10).

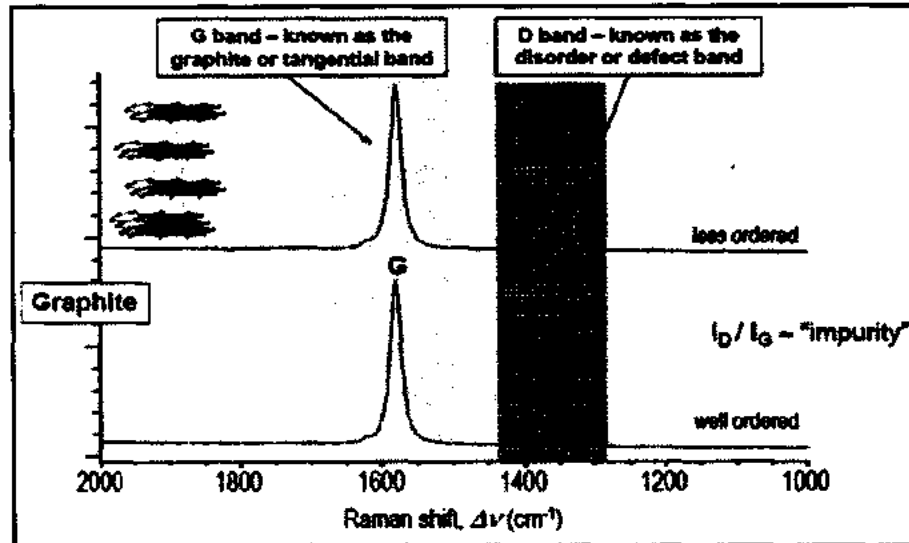


Figure 3-10: Raman spectra of graphene for a less ordered (top) and well-ordered (bottom) structure showing how D peak grows with increasing defects [92]

3.4 Dielectric Properties Measurements

The Electrical properties of the Graphene Nanoplatelets samples can be measured using LCR Meter over a specific frequency range.

3.4.1 What is LCR meter?

A LCR meter is an instrument used to compute the inductance, capacitance and, resistance of a sample. Inductance (L) is defined as when a current is passed through a conductor, it induces a voltage proportional to the rate of change in current in the conductor. In Electronics, capacitance (C) is the capacity of a body to store (or separated) an electrical charge for a given electric potential. The electrical resistance of an electrical element measures its opposition to the pathway of an electric current.

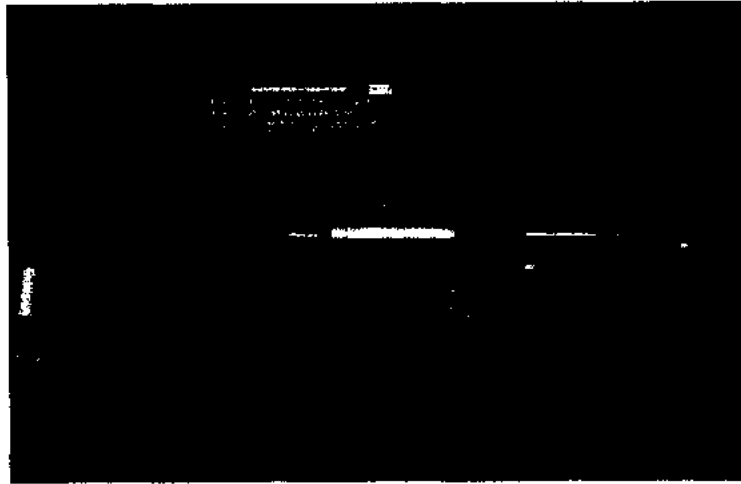


Figure 3-11: The 7600 Precision LCR Meter with LD-03 Dielectric Cell was designed to find Dielectric Constant and Dissipation Factor measurements [93]

3.4.2 Measurement Principle

The traditional LCR meter is a measurement system whose working principle is based on the “automatic balancing bridge method”, as shown in Fig.3-12.

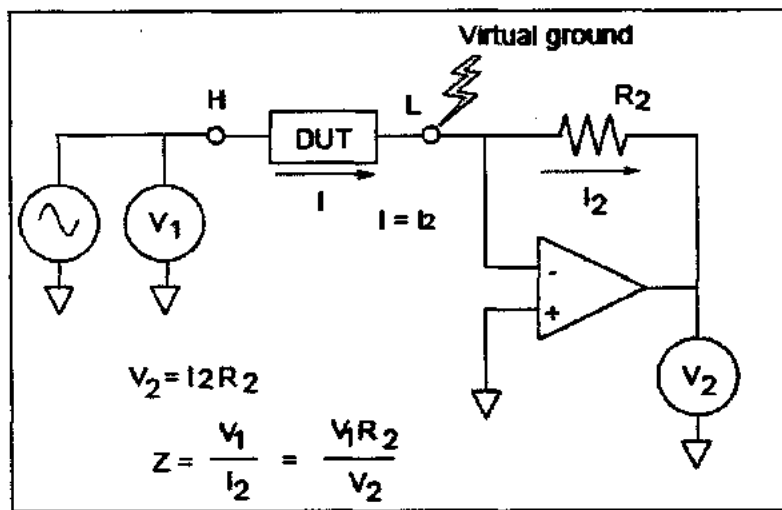


Figure 3-12: Principle Drawing of Automatic Balancing Bridge of LCR meter [94]

To facilitate an eclectic current haggard from end to end of a resistor (R), a high gain amplifier automatically regulates the gain level. The current flowing through the DUT (Device under Test) is always equal to resistor (R). It means that the L-side end potential of DUT always equal to virtual ground level. At this moment, impedance value Z_x of the DUT can be calculated from the input voltage E_1 , the output voltage E_2 and feedback resistance R as given below [95]:

$$Z_x = R * E_1 / E_2 \text{-----} (3)$$

$$E_1 = |E_1| \cos\theta_1 + |E_1| \sin\theta_1 \text{-----} (4)$$

$$E_2 = |E_2| \cos\theta_2 + |E_2| \sin\theta_2 \text{-----} (5)$$

At this stage, phase angles θ_1 of E_1 and θ_2 of E_2 are calculated at the same time, and Z_x is calculated from above eq. (4) and then capacitance and dissipation factor are determined [95, 96].

3.4.3 Working of LCR meter

The sample in the form of pellet is sandwiched between homemade two probe (electrodes) assemblies of LCR meter. An AC voltage is applied between the electrodes to find electrical properties of the sample. The voltage (V) across, and the current (I) through the sample are monitored by LCR meter. From the ratio of voltage and current, the meter can calculate the magnitude of the impedance (i.e. opposition offered by a current when it flows through a circuit). Then from impedance we can also find dissipation factor (D.F.) by dividing real part of impedance to imaginary part of impedance [95, 97].

USES

- ▶ It is used in production Testing of LCR Components
- ▶ It can be used for frequency Response, Component & Sensor Characterization
- ▶ It can be used for Component Screening
- ▶ It is also used for Material Testing
- ▶ It is also used in Quality Assurance Testing
- ▶ It is useful to calculate Dielectric Constant by means of Standard Test Cell [97, 98].

CHAPTER NO.4

4 RESULTS AND DICUSSIONS

4.1 Structural Analysis

XRD pattern of un-annealed and annealed samples of GNPs in range of 2θ (20° - 80°) are displayed in Fig (4-1). The two prominent diffraction peaks at 2θ values as 27.1° (002) and 55.2° (004) in XRD patterns are matched with the standards peaks of hexagonal graphite phase corresponds to JCPDS card No. (41-1487). No extra impurity phases are detected. In Fig (4-2) a high intensity and broad diffraction peak of (002) plane positioned at 27.1° represents the nanoscale crystallite size of GNPs samples.

XRD pattern presented in Fig (4-2) has revealed a shift in diffraction peak (002) in both direction of angle 2θ . This shift is due to variation in lattice parameters (a, c) of GNPs which have been calculated from the XRD data using Eqs. (2) & (3) [99].

$$a = \frac{\lambda}{\sqrt{3} \sin \theta_{100}} \text{----- (2)}$$

$$c = \frac{\lambda}{\sin \theta_{002}} \text{----- (3)}$$

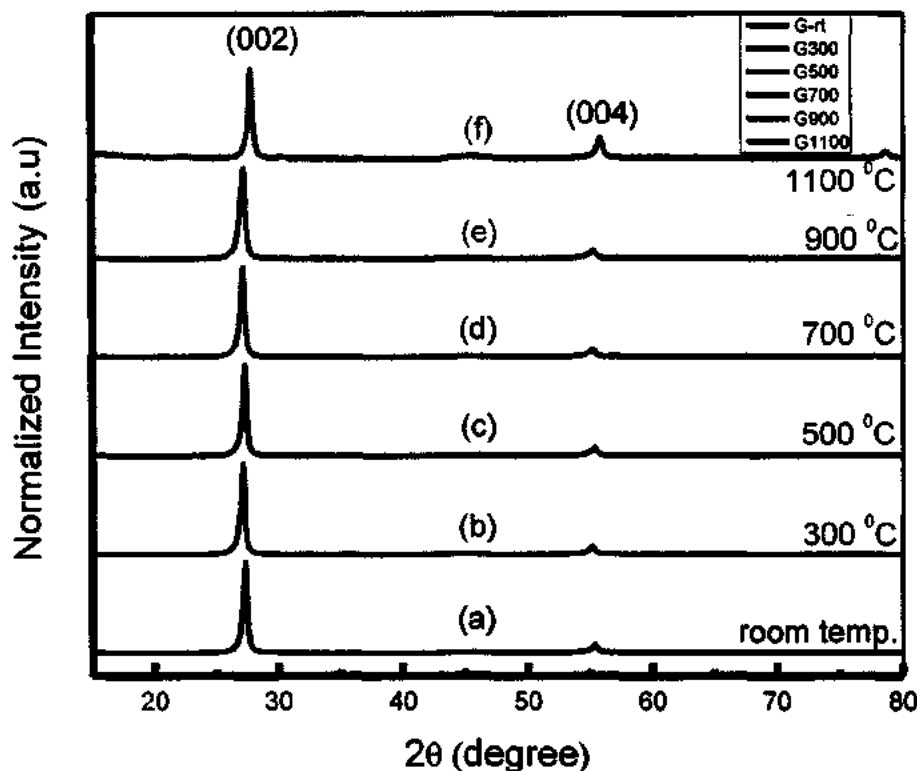


Figure 4-1: XRD pattern of GNPs samples (a) G-rt, (b) G300, (c) G500, (d) G700, (e) G900 and (f) G1100 annealed from 300 to 1100 °C for 1 hour in vacuum.

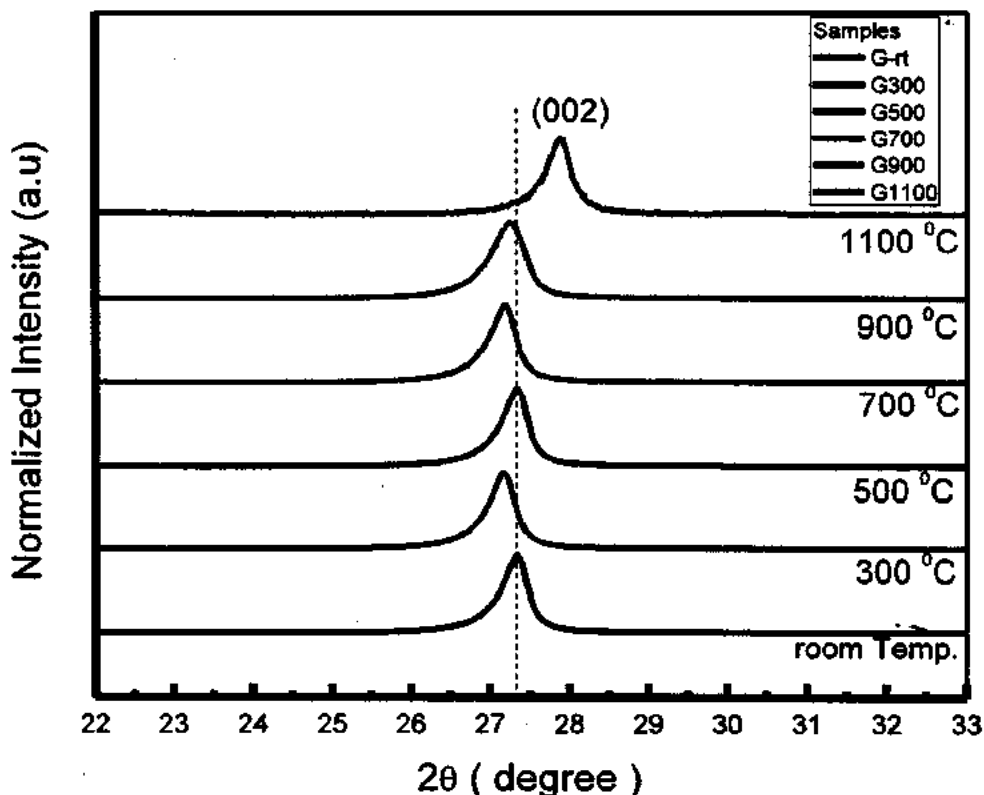


Figure 4-2: Extended XRD pattern of GNPs samples for (002) plane

For annealed samples G300, G700 and G900, diffraction peak (002) is shifted in lower value of angle (2θ) due to increase in lattice parameter values (a , c) as shown in Table 4-1. While for annealed samples G500 and G1100, diffraction peak (002) is shifted toward higher value of angle (2θ) due to reduction in lattice parameters values as illustrated in Table 4-1. This variation in lattice parameter and increased crystallite size produces a lattice strain in the crystal structure. This may be described on the basis of defects existing in the sample.

4.1.1 Calculation of FWHM, d-spacing, grain size, and number of layers

Table 4-1: Calculation of FWHM, d-spacing, particle size, intensity (cps) and no. of layers for (002) planes of GNPs samples.

Samples	2θ (002) Degree	FWHM rad.	d_{002} - spacing [Å]	Lattice parameters		Intensity (cps)	Grain Size (nm)	No. of layers
				a (nm)	c (nm)			
G-rt	27.1885	0.3346	3.27997	0.242	0.6550	28298	24	73
G300	27.1774	0.3739	3.28127	0.243	0.6554	27255	22	66
G500	27.3276	0.3542	3.26358	0.241	0.6520	28591	23	70
G700	27.2086	0.2558	3.27758	0.242	0.6547	25396	31	96
G900	27.2486	0.2755	3.27287	0.241	0.6540	25208	29	90
G1100	28.4998	0.1968	3.20034	0.227	0.6257	1259	41	128

Table 4-1 has also displayed a noticeably decrease in the d_{002} and FWHM values of (002) peaks during the thermal annealing of samples from 300-700 °C. This might be happened due to the removal of intercalated water molecules and defects [100] which demonstrate that degree of crystallinity of annealed samples is increased. However during annealing of G1100 at 1100 °C FWHM has become squatter due to increase in grain size (from 22 nm to 41 nm) and a sharp decrease in peak intensity (From table 1) shows poor crystallinity of annealed samples due to breaking of in-plane carbon bond (C=C).

From the XRD data d_{002} -spacing, grain size and no. of layers of all samples have been calculated as shown in Table.4-1 using Eqs. (4), (5) and (6).

$$d_{002} = n\lambda / \sin\theta_{002} \text{-----} (4)$$

Further, Grain size L_c (stacking height) is also obtained from XRD data by applying Debye-Scherer Equation to carbon materials [101-104].

$$L_c = 0.890 \lambda / \beta \cos \theta_{002} \text{-----} (5)$$

Where $k=0.89$ Scherer constant for GNPs and β is called Full Width at Half Maximum (FWHM).

From Scherer's equation, the number of GNPs layers (N) can be calculated by applying the equation given below [103-106]

$$N = L_{002} / d_{002} \text{-----} (6)$$

Fig.4-3 and Fig.4-4 show a variation in d-spacing and FWHM of GNPs samples with increasing temperature. As temperature increases, value of d-spacing decreases from 3.28 to 3.200 nm and FWHM from 0.374 to 0.197 Å attributed to the removal of intercalated water molecules [42]. Fig.4-5 and Fig.4-6 show an increase in grain size from 22 to 41 nm and no. of layers from 66 to 128 of GNPs with increasing temperature from 300 to 1100 °C. This confirms the multilayer platelets structure of our samples (> 10 layers). The chief driving force to create this large grain structure at the expense of small one's is due to the process of nucleation and the variation in inner energy between the strained and unstrained material [67].

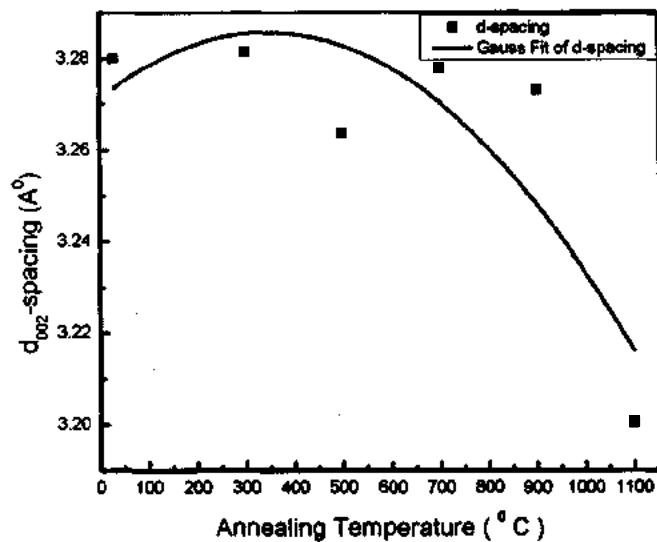


Figure 4-3: Variation in d-spacing d_{002} of GNPs with increasing Temperature

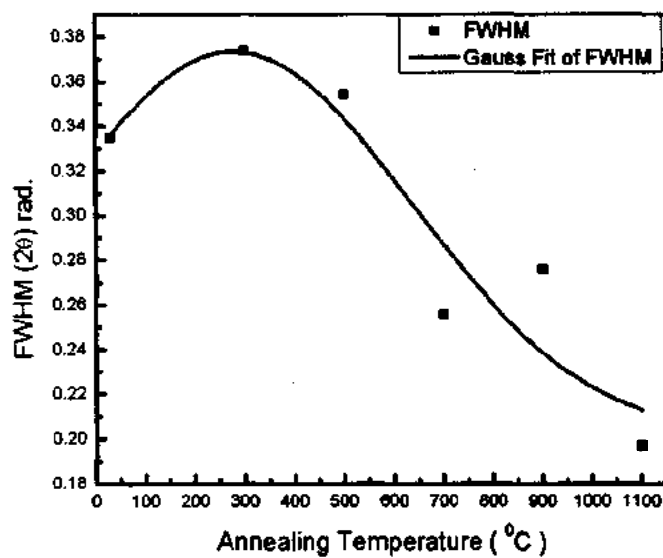


Figure 4-4: Variation in FWHM of GNPs with increasing Temperature

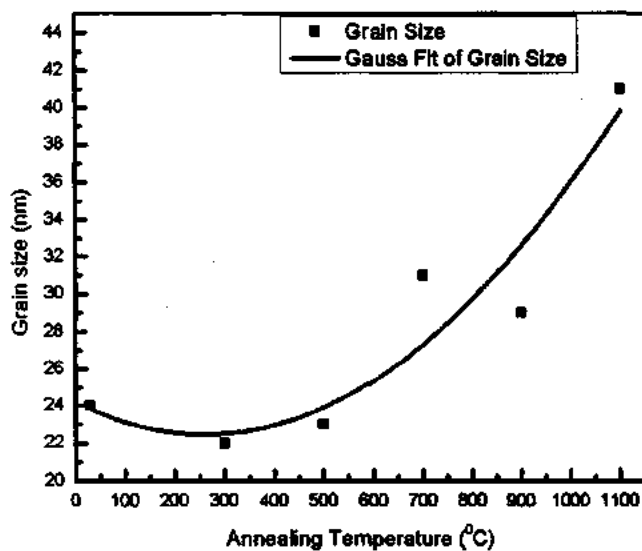


Figure 4-5: Variation in Grain Size of GNPs with increasing Temperature

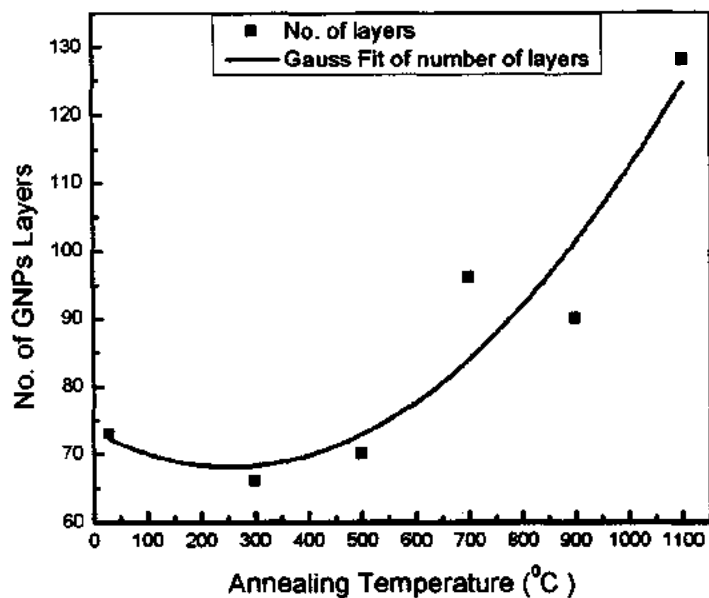


Figure 4-6: Variation in number of GNPs layers with increasing Temperature

4.2 Analysis of Raman Spectra

The Raman spectra of Grt, G300, G500, G700, G900 and G1100 have shown in Fig.4-7. The Raman spectra of the un-annealed (Grt) and annealed samples of GNPs have displayed a G peak at 1604 cm^{-1} , a D peak at 1374 cm^{-1} and a 2D peak at 2751 cm^{-1} . The G peak is a Raman signature of graphitic sp^2 materials and appears due to C-C broadening of all pairs of sp^2 carbon atoms in both chains and rings [108]. The D band is the result of breathing modes of sp^2 atoms in rings and an indication of defects introduced in GNPs [109]. The defects could be edges, dislocations, cracks or vacancies in the sample. Vacuum thermal annealing has been implemented to remove these defects.

The Raman spectrum of GNPs of 2D band is the result of a two phonon double resonance Raman process. This band is normally used to estimate the number of layers due to sensitiveness to the number of graphene layers [110-112]. The intensity ratio I_G/I_{2D} has a good connection with the number of graphene layers present. From table 4-2, it is clear that the I_G/I_{2D} ratio of our samples is ranging 1.5-1.95, with average 1.75 (> 10 layers) which is greater than the value ($I_G/I_{2D} \sim 1.03$) for few-layered graphene (2-10) processing by Arc-Discharge method [113]. This shows that our samples have multilayer structure (> 10 layers) which is also confirmed by XRD data.

Raman spectra has revealed that as the samples are annealed from 300 to 1100 °C, a decrease in frequency 8 cm^{-1} (Red shift) for D and G band and 7 cm^{-1} (Red shift) for 2D band is observed as shown in table 4-2. Basically the down shifted (red shift) means that frequency of

phonons interacting with incident photon is decreased, possibly reasons may be annealing, strain and structural changes in the material [114, 115].

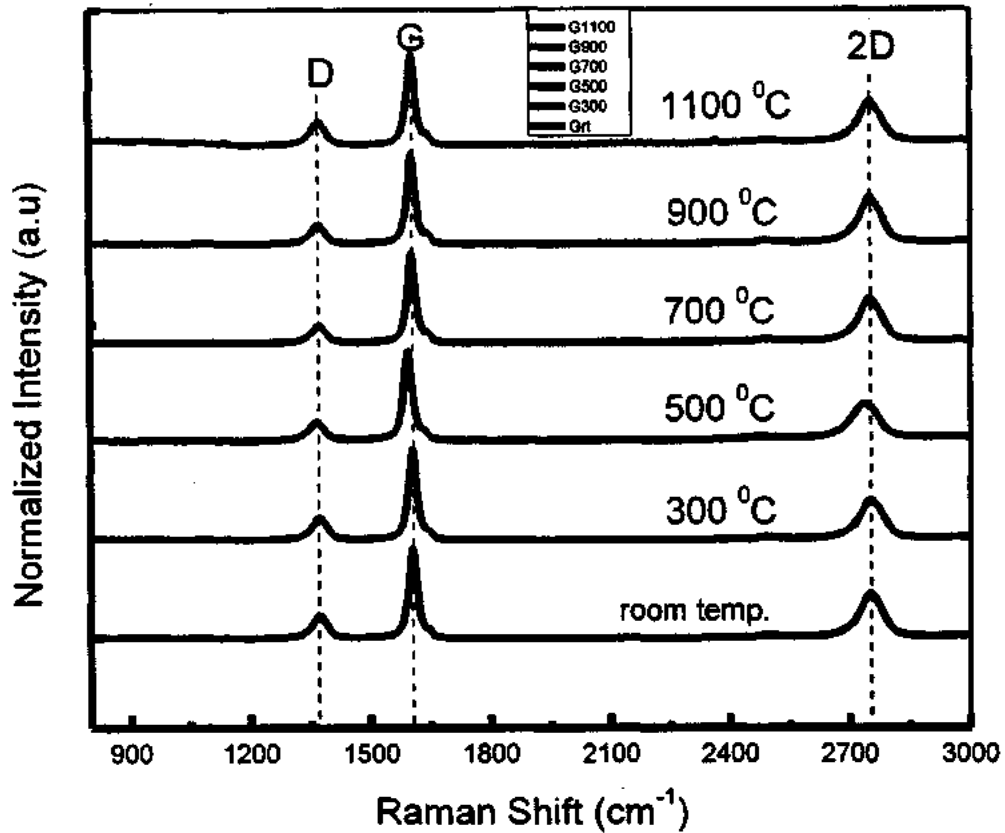


Figure 4-7: Raman spectra of the GNPs samples annealed at 300-1100 °C, showing D, G and 2D bands

Table 4-2: Calculations of peak position of D, G, 2D bands and peak intensity ratio I_D/I_G of GNPs annealed at 300-1100 °C

Sample	D-band position (cm ⁻¹)	G-band position (cm ⁻¹)	2D-band position (cm ⁻¹)	D (intensity)	G (intensity)	2D (intensity)	I_D/I_G (Defect ratio)	I_G/I_{2D} (Layers no. ratio)
G-rt	1374	1604	2751	16050	42065	24651	0.3815	1.70
G300	1374	1604	2751	16910	45946	24361	0.3680	1.89
G500	1374	1604	2751	14023	40455	20742	0.3466	1.95
G700	1371	1604	2749	14727	46898	26826	0.3140	1.75
G900	1371	1604	2749	15572	47670	27868	0.3266	1.71
G1100	1366	1596	2744	9215	16827	11529	0.5476	1.50
Red Shift	8	8	7					

Table.4-2 has also showed that I_D/I_G (Disorder/order) ratio (defect) is first decreased from 0.368 to 0.314 with increase in temperature from 300 to 700^oC and then abruptly increased from 0.314 to 0.5476 with increase in temperature from 700 to 1100^oC. A decrease in defect ratio up to 700 ^oC, may be due to removal of defects (intercalated water molecules) while a large increase in the disordering ratio in temperature range 700-1100^oC is due to in-plan bond cracking (C=C) of GNPs. These results are in accordance with XRD data. I_D/I_G intensity ratio of G700 is lowest, while G1100 has highest value as illustrated in Fig.4-8. Therefore, the quality of GNPs have improved as the temperature is increased from 300 to 700^oC and then decreased sharply as the temperature is increased from 700 to 1100^oC.

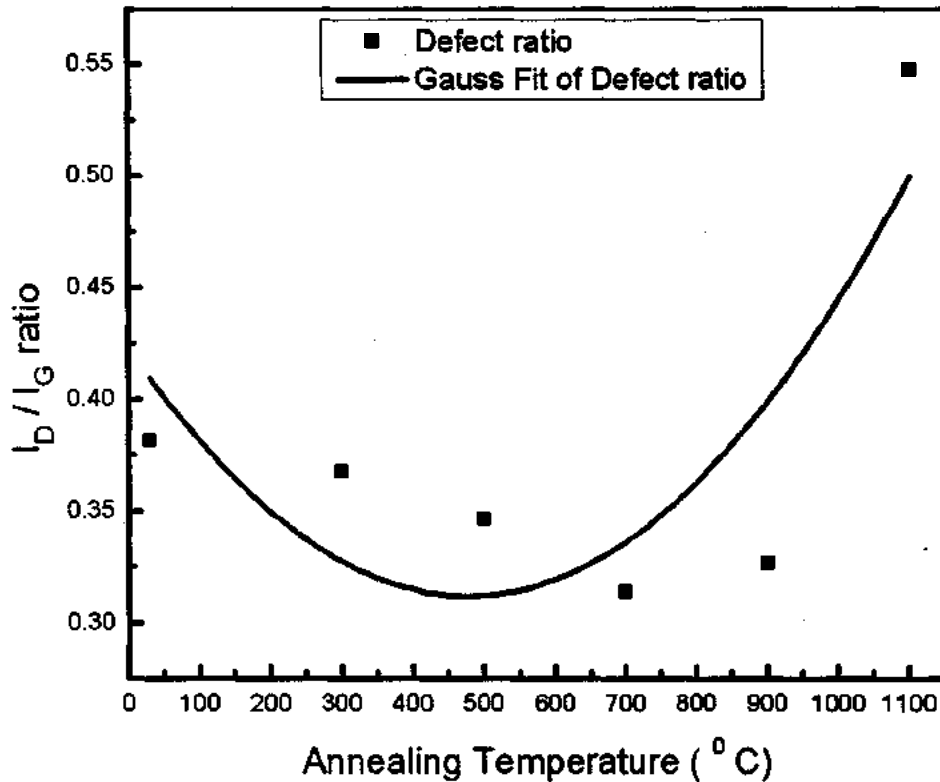


Figure 4-8: Variation in Defects (Peak intensity ratio I_D/I_G) of GNPs with increasing Temperature

4.3 Morphology of Graphene Nanoplatelets

Fig. 4-9 has displayed the FE-SEM images and EDX pattern of un-annealed Grt and annealed samples G300, G700 and G1100 of GNPs. We annealed three samples under vacuum condition at 300 °C, 700 °C, and 1100 °C. The GNPs annealed at 700 °C is marginally larger than those annealed at 300 °C and have uneven edge as a result of ceaseless accumulation of small carbon clusters. At an annealing temperature of 1100 °C, the GNPs grow affectedly bigger but with reduced quality due to Smoluchowski ripening, which describes the diffusion of small islands and relaxation of large islands to equilibrium [116].

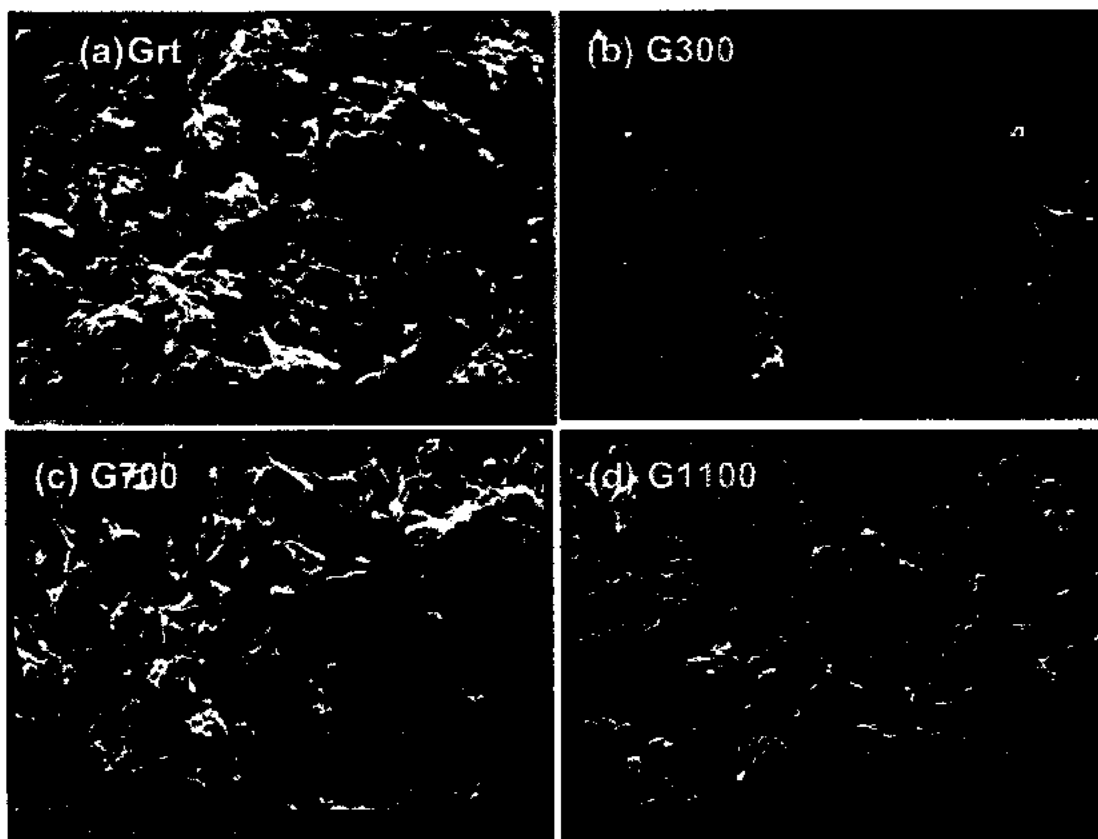


Figure 4-9: FE-SEM images (a) un-annealed GNPs (b) GNPs annealed at 300 °C (c) GNPs annealed at 700 °C and (d) GNPs annealed at 1100 °C for 1 hour

The FESEM images have also indicated that their platelet like overlapped morphology is increased by increasing temperature from 300 to 1100 °C. Overlapping and agglomeration of GNPs are due to strongly Van der Waals forces. This enhancement in overlapped morphology leads to an increase in the particle size as in line with XRD data. To obtain ideal sizes and high quality of GNPs, this investigation offers new information about the influence of

annealing temperature on GNPs and could be favorable to well controlling the growth of GNPs.

4.3.1 EDX analysis

EDX pattern in fig. 4-10 reveals that as-prepared sample Grt and heat treated samples G300, G700 and G1100 are composed of only carbon element with atomic/weight percentage 100 and no other impurities are present in the samples. EDX pattern also has displayed that the higher annealing treatment of GNPs samples leads to no change in percentage of carbon atoms.

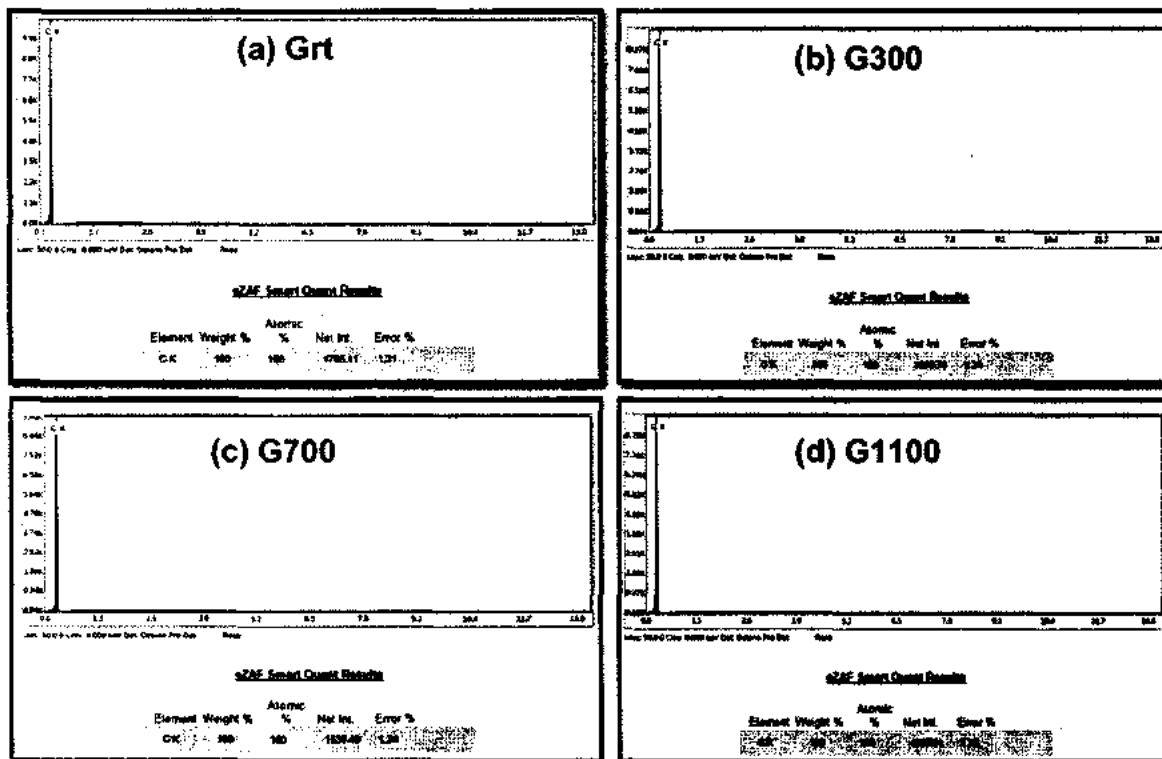


Figure 4-10: EDX spectra of (a) un-annealed GNPs (b) GNPs annealed at 300 °C (c) GNPs annealed at 700 °C and (d) GNPs annealed at 1100 °C for 1 hour in vacuum

4.4 Measurement of Dielectric Properties

Generally, the complex relative permittivity ϵ of materials is known as

$$\epsilon = \epsilon' + j \epsilon'' \text{-----} (7)$$

The real part of effective permittivity ϵ' is a measure of the ability to storage the external electromagnetic energy in the material, which is due to electric polarization effects and dielectric relaxation involving unpaired point defects, bound charges and polarized interfaces [117, 118]. The imaginary part of effective permittivity ϵ'' relates to ability of a material to dissipate the energy from an external electromagnetic field and convert it into heat, which is mainly due to the presence of free electrons in the material [119].

Prepared pellets of GNPs of diameter 13 mm and thickness 3 mm are used to measure dielectric properties using LCR meter. Capacitance (C) and dissipation Factor (D) of all the pellets of GNPs were calculated with LCR meter in the frequency range of 100 Hz to 5MHz.

4.4.1 Variation in dielectric constant with frequency

The dielectric constant (ϵ') was calculated from the equation [145]

$$\text{Dielectric Constant} = \epsilon' = (t \times C_p) / (A \times \epsilon_0) \text{-----} (8)$$

Where t is thickness of the pellets, C_p is the corresponding parallel capacitance acquired experimentally, A is the area of the pellets and ϵ_0 is permittivity of vacuum ($\epsilon_0 = 8.854 \times 10^{-12}$ F/m (farads per meter)).

The variation in dielectric constant due to increase in frequency for GNPs is represented in figure 4-11. This Fig. has revealed that dielectric constant is extremely high ranging from 10^{12} to 10^{13} at low frequencies and then decreases at higher frequency and eventually becomes constant. It is noticed from the figure that the maximum dispersion of dielectric constant take place when frequency changes from 1kHz to 10 kHz. This is due to the existence of different forms of polarization mechanisms like electronic, ionic orientation and space charge polarization [120]. Koops suggested that the effect of grain boundary on dielectric constant is very high at low frequencies [119]. In space charge polarization, when electric field is applied on the dielectric material, charge carriers gather at the grain boundaries and dipole moments are created [121]. When the frequency of the applied electric field is further increased than a certain limit, space charge carriers can not follow the variations of applied field and their directions lag behind the field. Hence polarization decreases causing a decrease in dielectric constant at higher frequency [122]. This type of Interfacial polarization is called Maxwell-Wagner-Sillars polarization. This polarization is the main reason of improvement in dielectric permittivity of GNPs at low frequency [123]. A

slight hump in dielectric constant is observed for all samples at low frequency range 1-10 k Hz [131].

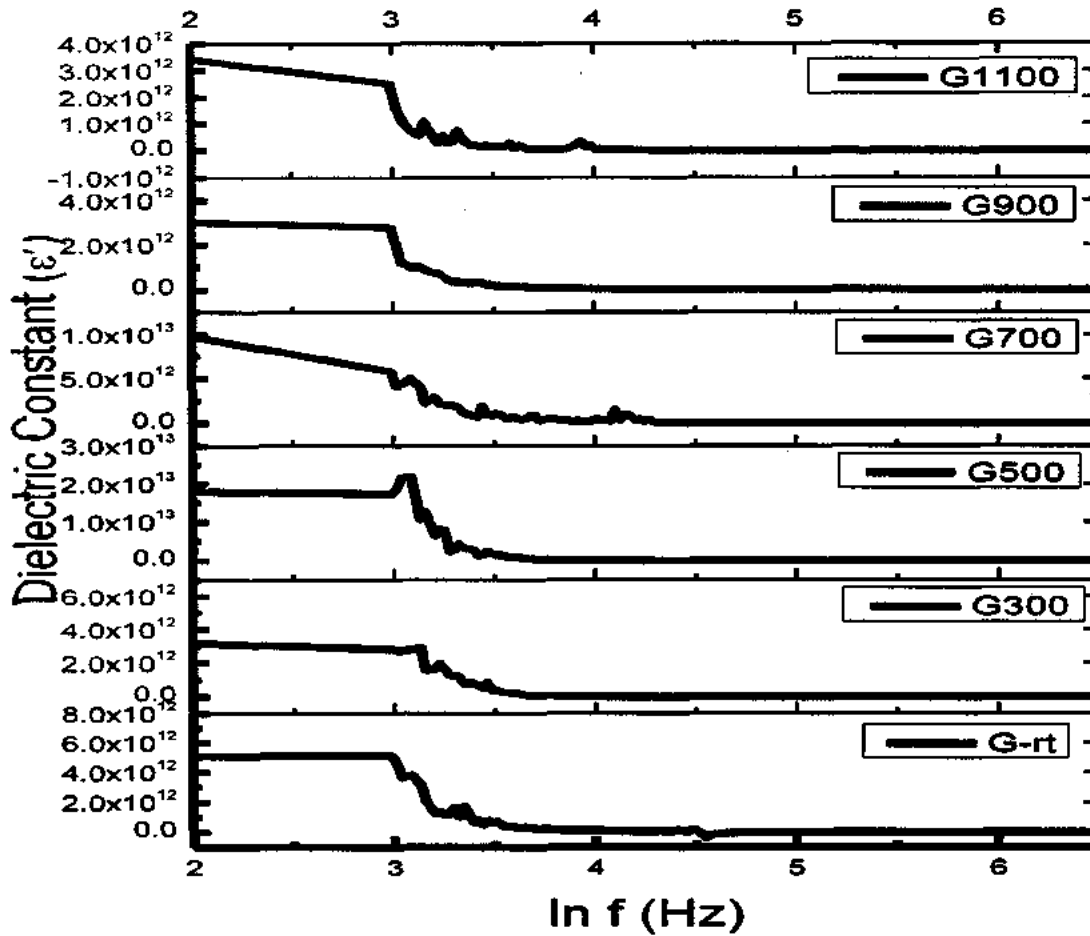


Figure 4-11: Variation in dielectric constant as a function of frequency of GNPs samples annealed at 300-1100 °C

4.4.2 Variation in dielectric constant with temperature

The change in dielectric constant with increasing annealing temperature for GNPs samples is shown in figure 4-12 at constant frequency 100 Hz. Dielectric constant of nanostructured materials depends on many factors like frequency, annealing temperature, grain size, grain boundaries, defects, porosity etc. Figure 4-11 displays that almost all samples of GNPs have high dielectric constant ranging from 10^{12} to 10^{13} at fixed frequency. At fixed frequency 100Hz, the high value of dielectric constant of Grt and G1100 is mainly due to variation in defects which are strongly dependent on temperature [124]. Due to these defects, interfacial polarization increases due to gathering of space charge carriers at the grain boundaries which results very high dielectric constant of GNPs [125-127]. As temperature

increases from 300 to 700°C, the values of dielectric constant has decreased due to decrease in volume of defects and then abruptly increased from 10^{12} to 10^{13} with increase in temperature from 700 to 1100°C due to increase in density of defects. These results are well agreement with Raman defects ratio (I_D/I_G) as shown in Fig. 4-8. In-plan bond breaking (C=C) and sp^2 - sp^3 conversion in GNPs may be the main source of these defects.

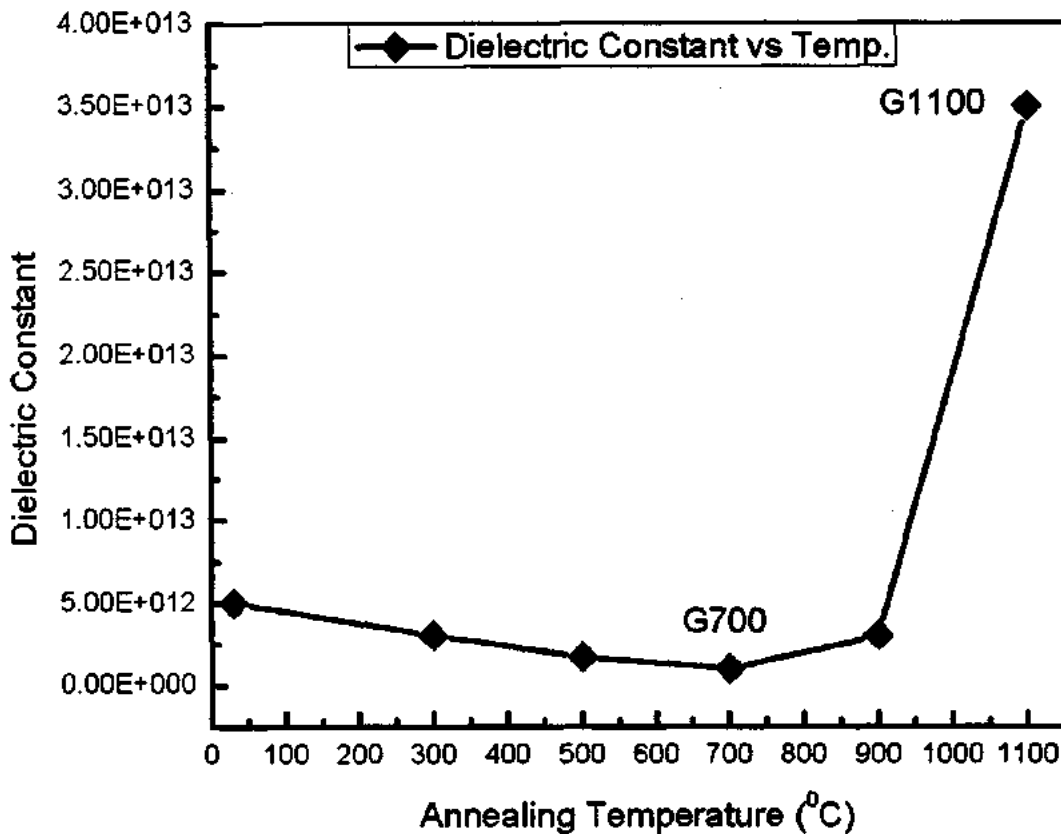


Figure 4-12: Variation in dielectric constant of GNPs with increasing temperature

4.4.3 Variation in dielectric loss with frequency and temperature

The dielectric loss (ϵ'') was calculated from the multiplication of ϵ' with the dissipation factor D obtained experimentally.

$$\text{Dielectric Loss} = \epsilon'' = (\text{dissipation factor}) * (\text{permittivity of vacuum}) = D * \epsilon_0 \text{ ----- (9)}$$

Fig. 4-13 displays the change in dielectric loss as a function of frequency for annealed GNPs at temperatures range of 300-1100 °C. All annealed samples show high values of dielectric from 100 Hz to 1k Hz frequency range and then decreases at higher frequency. The initial low value of dielectric loss vs. frequency is exceptional as polarization does have changing time response capability to the frequency of an applied field. At frequency 100 Hz, dielectric loss is small due to molecules having large relaxation time with delayed polarization

processes. Different causes are assumed to be intricate in such polarizations i.e., electronic, ionic, and space charge displacements [128-130].

A peaking nature in dielectric loss is observed for all samples at low frequency range 100-500 Hz which is explained by A.Thakur [131], according to this theory, peaks observed when jumping frequency of electrons is equivalent to the applied field frequency i.e. $\omega \tau = 1$ Where τ represents the relaxation time which is inversely proportion to the jumping probability.

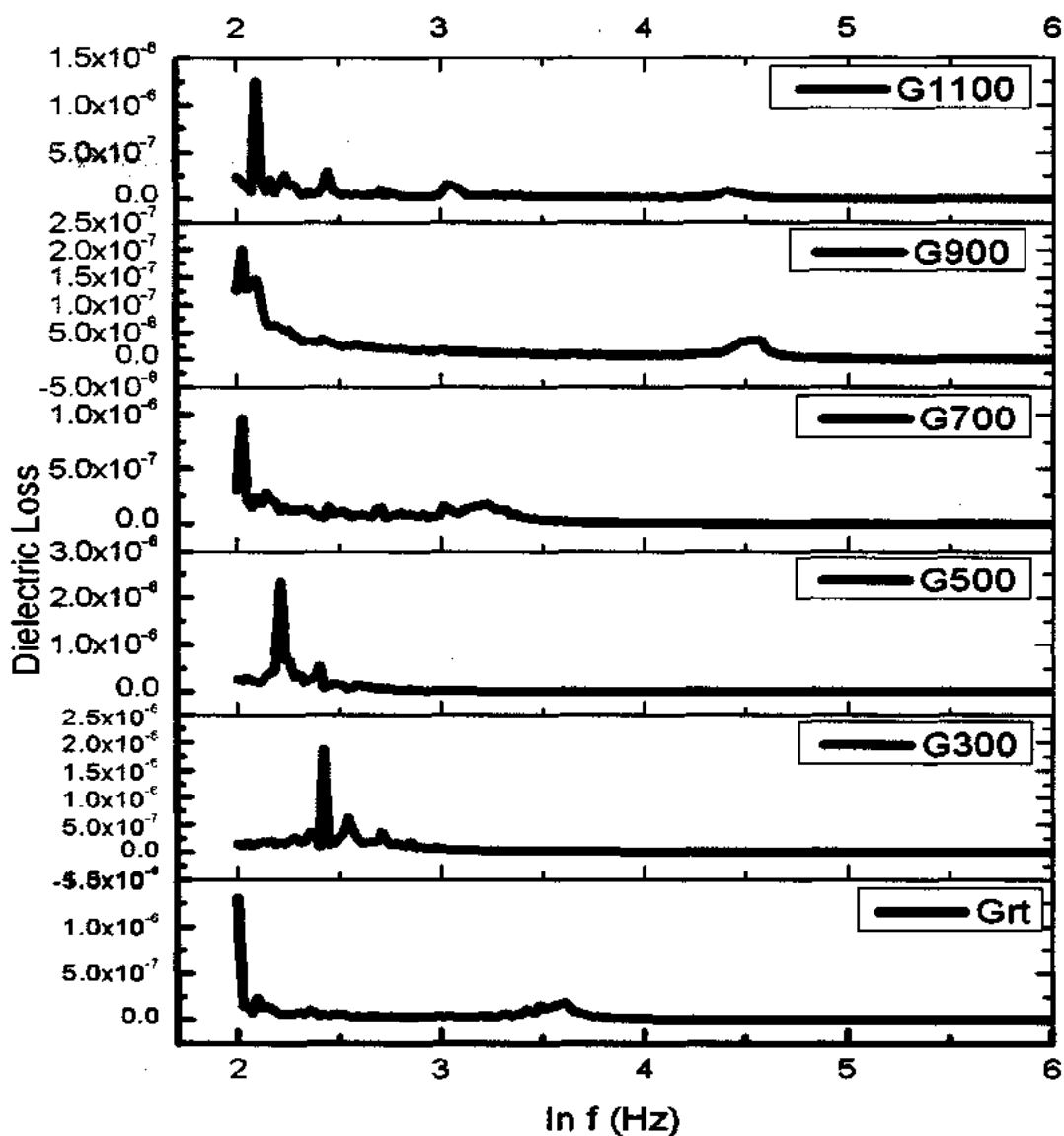


Figure 4-13: Variation in dielectric Loss as a function of frequency of GNPs samples annealed at 300-1100 °C

At high frequencies (500 Hz - 5 M Hz), the decrease in Dielectric loss with frequency can be described by Koop's Theory [119]. This theory explains that the structure of a dielectric material acts as an inhomogeneous medium of the Maxwell-Wagner type [133].

4.4.4 Variation in Dielectric loss tangent with frequency and temperature

The dielectric loss tangent was calculated from the equation [146]

$$\text{Tan } \delta = \varepsilon''/\varepsilon' \text{ ----- (10)}$$

The variation of dielectric loss tangent ($\tan\delta$) as a function of frequency for GNPs has represented in figure 4-14(a). The value of dielectric loss tangent is almost zero at low frequencies up to 10^4 Hz. At higher frequencies from 10^5 to 10^6 Hz, these materials exhibit almost negative dielectric loss which suggests that GNPs are lossless materials (having no dissipation of electrical or electromagnetic energy) at higher frequencies.

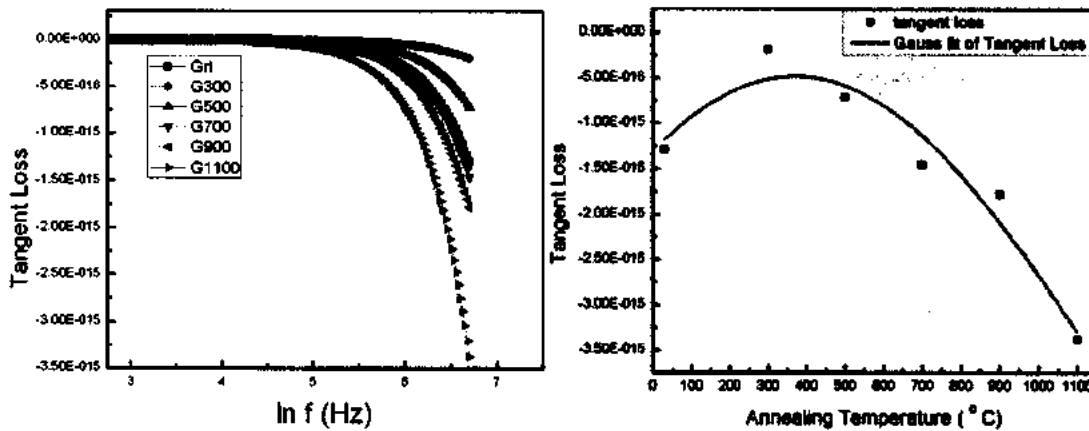


Figure 4-14: Variation in Dielectric loss tangent, as a function of (a) frequency and (b) temperature of GNPs samples annealed at 300-1100 °C

Dielectric loss tangent of nanostructured materials depends on frequency, grain size, grain boundaries, defects, porosity etc. The variation in Dielectric loss tangent with annealing temperature can be explained with change grain size. From Fig. 4-14(b), it can be seen that the sample G300 annealed at 300 °C with grain size 22 nm (from XRD data) has small negative value of dielectric loss tangent while sample G1100 with a grain size of 128 nm (from XRD results) annealed at 1100 °C has a large negative value for the dielectric loss tangent ($\tan \delta$). These results have revealed that the dielectric loss tangent decreases as annealing temperature (grain size) increases. This increase in grain size results a decrease in the number of interface boundaries and also lesser volume of defects that results different type of polarizations and hence a decrease in dielectric loss tangent [134].

4.4.5 Variation in A.C conductivity with frequency

The AC conductivity was calculated from the equation given below [135]

$$\sigma_{ac} = 2\pi f \epsilon_0 \epsilon' \tan\delta \text{----- (11)}$$

Where $\tan\delta = \epsilon'' / \epsilon'$ (eq. 10)

The variation of A.C conductivity (σ_{ac}) as a function of frequency for GNPs has represented in figure 4-15. The enhancement of A.C conductivity was explained by many authors on the basis of excess ion vacancies due to the high conduction of the space charge layer. The A.C conductivities of all annealed samples (G300, G500, G700, G900 and G1100) is low as 0.001 S/m at low frequency region 100 Hz and then increases with increase in frequency from 1k Hz to 100 kHz according to power law, which states that σ_{ac} is directly proportional to AC frequency as shown in Fig.8a. At higher frequencies above 0.1M Hz, there is decrease in σ_{ac} which can be described due to polarons. A polaron has two types i.e., large and small which depends on how its radius equates to the lattice constant of the material. The conductivity of a large polarons is due to band mechanism at all temperatures and decreases with increase in frequency while the small polarons conduct in bands at certain temperature, and their conductivity increases with increase in frequency [136, 137].

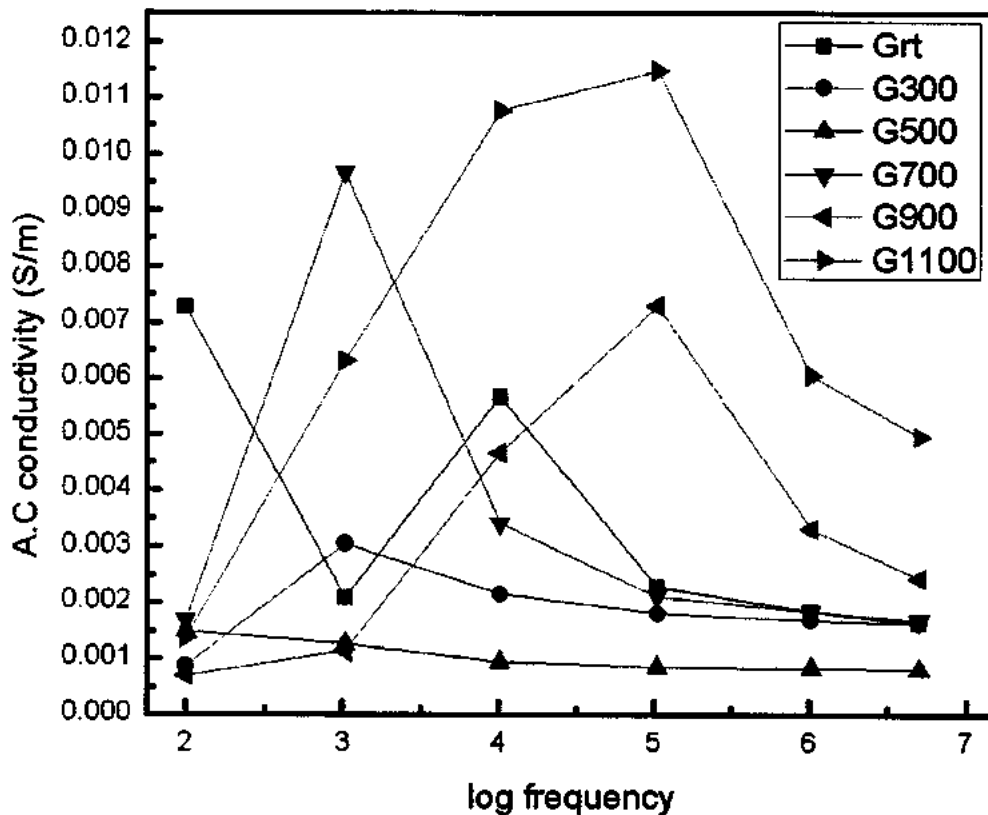


Figure 4-15: Variation in A.C Conductivity with frequency of GNPs samples annealed at 300-1100 °C

A peaking nature in A.C conductivity (σ_{ac}) against frequency is observed for all samples at frequency range 10^3 - 10^5 Hz as shown in fig. 4-15 which is described by Thakur [131]. This theory states that the peaks are detected when the jumping frequency of electrons is equivalent to the applied field frequency i.e. $\omega \tau = 1$. It is clear that the relaxation peak height increases with increasing in grain size. The frequency dependent data showed that maximum value of σ_{ac} is due to large grains size rather than surface conduction or grain boundary [138, 139]. Fig.4-15 shows that value the σ_{ac} of G1100 is maximum (0.012 S/m) due to large grain size 41nm, while G500 sample has lowest value (0.001 S/m) due to smallest grain size 22 nm.

4.4.6 Variation in A.C conductivity with temperature (defects)

In graphene, grain boundaries are non-hexagonal rings defects at the boundaries between two domains with different crystallographic orientations [140–143]. These defects can disturb the movement of delocalized π -electrons and efficiently disperse the electrons which normally reduce the conductivity of a material [141–143].

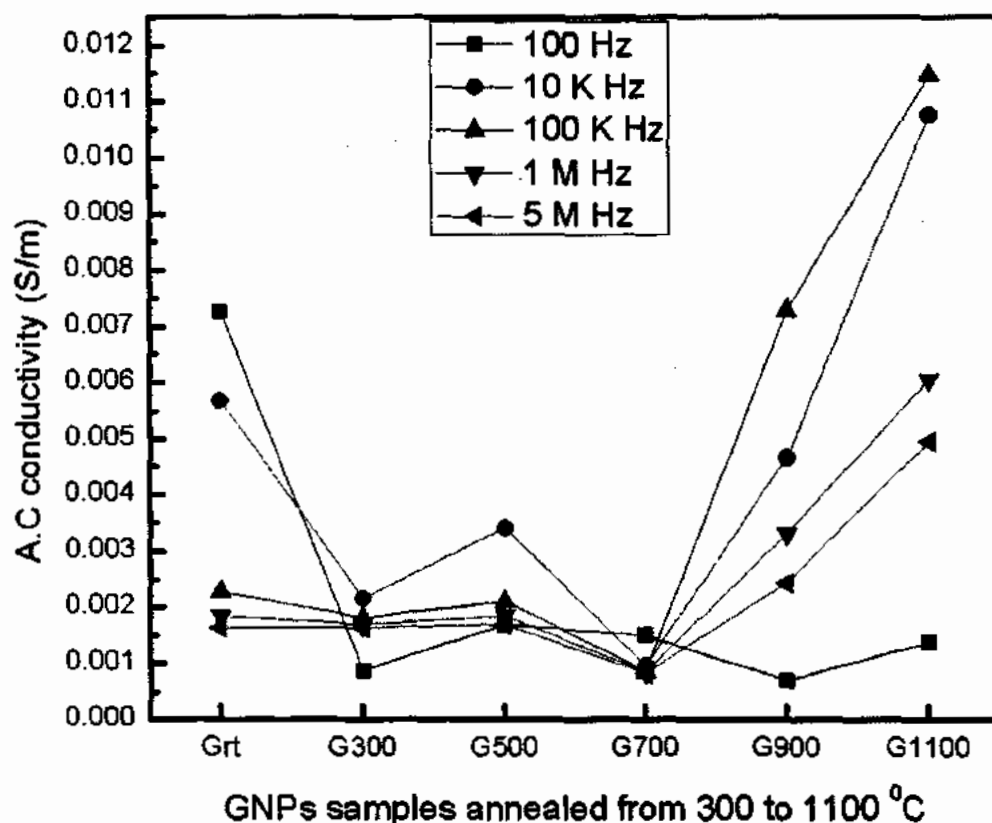


Figure 4-16: Variation in A.C conductivity with increasing Temperature at Fixed Frequency

Our results have revealed that defects improve the AC conductivity of GNPs which is counter-intuitive as reported in [141]. Fig. 4-16 clearly shows that there is significant change

in AC conductivity of GNPs with increasing temperature from 300 to 1100 °C. High value of σ_{ac} at room temperature (Grt) and 1100 °C (G1100) for all frequency ranges is due to the existence of defects. These line or dislocation like defects serves as trapping center of electrons which increases the electrical conductivity of GNPs [140, 144]. As the temperature is increased, value of σ_{ac} is decreased due to reduction in defects until temperature range 700 °C as shown in Fig. 4-16. Above 700 °C, there is an increase in σ_{ac} which is due to large volume of defects as a result of C=C bond breaking [145]. This enhancement in conductivity with defects is well agreement with Raman defects ratio (I_D/I_G) and dielectric constant vs. temperature graph as shown in figure 4-8 and figure 4-12 respectively.

5 CONCLUSIONS

The prepared GNPs have been successfully annealed at different temperature to tune the physical properties. The structural study has clearly showed the improvement in the crystallinity, enhancement in grain size and number of graphene layers by annealing.

Raman spectra have revealed a decrease in frequency of D, 2D and G bands for all annealed samples. The intensity ratio I_G/I_{2D} of prepared samples have showed multilayer structure (> 10 layers) which is also confirmed by XRD data. The quality of GNPs has improved as the temperature is increased from 300 to 700 °C and then decreased sharply above 700 °C.

The FESEM images have indicated that during thermal annealing of GNPs, their platelet like overlapped morphology is increased. This enhancement in overlapped morphology leads to an increase in the particle size as in line with XRD studies. EDX patterns have revealed that the heat treated samples are contained only carbon atoms and no other impurities are present in the annealed samples.

Considerable variation in dielectric constant, dielectric loss and dielectric loss tangent of GNPs has been observed by annealing at fixed frequency. Similarly, AC conductivity of GNPs has significantly varied by increasing temperature and frequency.

Our results conclusively show that high-quality GNPs can be achieved by vacuum annealing at 700 °C temperature and their high dielectric constant and enhanced electrical conductivity can be used to fabricate high dielectric-based electronic and energy storage devices.

6 REFERENCES

- [1]. Kroto, H.W., et al., *Nature*, Volume 318, 162 (1985).
- [2]. Krätschmer, W., et al., *Nature*, Volume 347, 354 (1990).
- [3]. Haddon, R.C., Brus, L.E., and Raghavachari, K., *Chem. Phys. Lett.*, Volume 131, 165 (1986).
- [4]. Chang, Raymond *Chemistry*, Ninth Edition. McGraw-Hill, pp.52 (2007).
- [5]. Jean-Noël FUCHS Mark Oliver GOERBIG, "Introduction to the Physical Properties of Graphene" Lecture Notes (2008).
- [6]. Mattias Mase, "Nanostructured Carbon Materials under Extreme Conditions" Lulea University of Technology, (2014).
- [7]. Heimann R.B., Evsyukov S.E., and Koga Y., *Carbon* 35, 1654 (1997).
- [8]. Dr. Ron Rusay Foundation, *Organic Chemistry, Chem226*, (2012)
- [9]. Chen, G. H.; Wu D.J., etc. *Polymer International*, Volume 50, 980 – 985(2001).
- [10]. Chung D.D.L., *Review Graphite, Journal of materials Science* 37, 1-15 (2002)
- [11]. Xiao, M.; Sun, L.; Liu, J.; Li, Y.; Gong, K. *Polymer*, Volume 43, 2245 – 2248(2002).
- [12]. Franklin, R.E. *Royal Society London A London*, 209, 196 (1951)
- [13]. Prof. Dr. Anke Krueger, *Universität Würzburg Institut für Organische Chemie Am Hubland 97074 Würzburg German* (2014).
- [14]. S. Mitura , K. Mitura , P. Niedzielski , P. Louda, V. Danilenko , *Journal of AMME*, Volume 16, 1-2 (2006).
- [15]. Timo Vehviläinen, "Hydrogen interaction with carbon nanostructures", *Aalto University publication series Doctoral Dissertations* (2012).
- [16]. "Diamond-like carbon films". (pdf) 2nd Ed., Retrieved (2006).
- [17]. M.G. Fyta, C. Mathioudakis¹, G. Kopidakis², P.C. Kelires, *Thin Solid Films* 482, 56–62 (2005)
- [18]. "Amorphous carbon". *IUPAC Compendium of Chemical Terminology (pdf)* (2nd Ed.). 1997. Retrieved (2006).
- [19]. Kroto, H. W., Heath, J. R., O'Brien, S. C., Curl, R. F., and Smalley, R. E. *Nature* Volume 318, 162–163(1985).
- [20]. Iijima, S. *Nature*354 (November), 56–58 (1991).
- [21]. Novoselov, K. S., Geim, A. K., Morozov, S. V., Jiang, D., Zhang, Y., Dubonos, S. V., Grigorieva, I. V., and Firsov, A. A. *Science*, Volume 306, 666–9(2004).
- [22]. M.Inagaki, *New carbons*, Elsevier, (2000).
- [23]. Dresselhaus M.S., Dresselhaus G., Saito R., 'Nanotechnology in Carbon Materials', ed.

- G. Timp, AIP Press, p. 285–33(1999).
- [24]. Geim, A. K., Novoselov, K. S., Nature Materials, Volume 6, 183-191 (2007).
- [25]. Kroto, H.W., Heath, J.R., O'Brien, S.C., Curl, R.F. and Smalley, R.E. Nature, Volume 318, 162-163(1985).
- [26]. R. Kuzuo et al., Jpn. J. Appl. Phys. Volume 33, 1316 (1994).
- [27]. G. E. Scuseria., Chem. Phys. Lett. Volume 243, 193-198(1995).
- [28]. Prinzbach, H., Weller, A.; Landenberger, P., Wahl, F.; Worth, J., Scott, L.T., Gelmont, M., Olevano, D., von I., Nature, Volume 407, 60-63(2000).
- [29]. V. L. Kuznetsov, A. L. Chuvilin, Yu. V. Butenko, et al. 'Science and Technology of Fullerene Materials', edited by P. Bernuer, et al. pp. 105–110(1995).
- [30]. Timo Vehviläinen., "Hydrogen interaction with carbon nanostructures". Department of Applied Physics Aalto University publication series Doctoral Dissertations. ISBN 978-952-60-4470-5. 5 (2012).
- [31]. Wang et al., Nano Letters, Volume 9, 3137–3141(2009).
- [32]. Coville N.J., Mhlanga S.D., Nxumalo E.N., Shaikjee A., S. Afr. J. Sci.; Volume 107, Art. # 418, 15 (2011).
- [33]. Daniel R. Dreyer, Prof. Rodney S. Ruoff and Prof. Christopher W. Bielawski. Volume 49, Issue 49, 9336–9344 (2010).
- [34]. A. S. Mayorov, R. V. Gorbachev, S. V. Morozov, L. Britnell, R. Jalil, L. a. Ponomarenko, P. Blake, K. S. Novoselov, K. Watanabe, T. Taniguchi, and a. K. Geim, Nano letters, Volume 11, 2396–9(2011).
- [35]. Chen, J.-H., Jang, C., Xiao, S., Ishigami, M., and Fuhrer, M. S. Nature nanotechnology, Volume 3(4), 206–9(2008).
- [36]. Ado Jorio, Riichiro Saito, Gene Dresselhaus, and Mildred S. Raman Spectroscopy in Graphene Related System. Dresselhaus. KGaA, Weinheim. ISBN: 978-3-527-40811-5
- [37]. Wang Haomin. "Growth and Characterization of two Dimensional Carbon Nanostructures". Doctoral Dissertations, National University of Singapore, (2009).
- [38]. Soldano, C.; Manmood, A.; Dujardin, E. Carbon, 48, 2127 (2010).
- [39]. Lee, C., Wei, X., Kysar, J. W., and Hone, J. Science, Volume 321, 385–8(2008).
- [40]. Geim, A. K. and Novoselov, K. S., Nature materials Volume 6(3), 183–191(2007).
- [41]. Bundy F.P., Bassett W.A., Weathers M.S., et al., Carbon, Volume 34,141–153(1996).
- [42]. McClure J. W., Phys. Rev. Volume 104, 666(1956).
- [43]. Slonczewski J. C. and Weiss P. R., Phys. Rev., Volume 109, 272(1958).

- [44]. Castro E. V., Novoselov K. S., Morozov S. V., Peres N. M. R., Lopes dos Santos J. M. B., Nilsson J., Guinea F., Geim A. K. and Castro Neto A. H., *Phys. Rev. Lett.*, Volume 99, 216802(2007).
- [45]. McCann E. and Fal'ko V. I., *Phys. Rev. Lett.*, Volume 96, 086805(2006).
- [46]. S. Latil and L. Henrard, *Phys. Rev. Lett.*, vol.97, pp.036803, (2006).
- [47]. Editorial, Elsevier Ltd. <http://dx.doi.org/10.1016/j.carbon.2013.08.038>. *Carbon*, Volume 65, 1–6 (2013).
- [48]. Ferrari A. C., et al., *Phys. Rev. Lett.* Volume 97, 187401(2006).
- [49]. Henriksen E. A., Nandi D. and Eisenstein J. P., *Phys. Rev.*, Volume 2, 11004 (2012).
- [50]. Taychatanapat T., Watanabe K., Taniguchi T. and Jarillo-Herrero P., *Nature Phys.*, Volume 7, 621(2011).
- [51]. Khodkov T., Withers F. D., Hudson C., Craciun M. F. and Russo S., *Appl. Phys. Lett.*, Volume 100, 13114(2012).
- [52]. Avetisyan A., Partoens B. and Peeters F. M., *Phys. Rev.*, Volume 81, 115432(2010).
- [53]. Lui C. H., Li Z., Chen Z., Klimov P. V., Brus L. E. and Heinz T. F. *Nano Lett.* Volume 11, 164 (2011).
- [54]. Koshino M and McCann. E., *Phys. Rev.*, Volume 79, 125443 (2009).
- [55]. Jang BZ, Zhamu A., *J. Mater Sci*; Volume 43, 5092–101(2008).
- [56]. Xulin Yang, Zicheng Wang, Mingzhen Xu, Rui Zhao, and Xiaobo Liu, *Materials & Design*, Volume 44, 74–80(2013).
- [57]. Cristina Ramirez, Filipe M. Figueiredo, Pilar Miranzo, P. Poza, and M. Isabel Osendi, *Carbon*, Volume 50(10), 3607–3615(2012).
- [58]. Wang Q., Wang C., Wang Z., Zhang J., and He D., *Applied Physics Letters*, Volume 91(14), 141902 (2007).
- [59]. King J. A., Klimek D. R., Miskioglu I., and Odegard G. M., *Journal of Applied Polymer Science*, Volume 128(6), 4217–4223 (2012).
- [60]. Caryn L. Heldt, et al. *Sensors and Actuators B: Chemical* Volume 181, 92–98 (2013).
- [61]. ZhouWang, ChengBingWang, QiWang, JunyanZhang, *Sensors and Actuators B: Chemical* Volume 181, 92–98 (2013).
- [62]. James Loomis, Ben King, Burkhead, Peng Xu, Nathan Bessler, Eugene Terentjev, and Balaji Panchapakesan, *Nanotechnology* Volume 23(4), 045501 (2012).
- [63]. Huang Wu and Lawrence T. Drzal, *Carbon*, Volume 50(3), 1135–1145 (2012).
- [64]. Dave Graber, NewTechs Product, davidgraber@newtechs-llc.com, (269) 986-4124 (2008).

- [65]. Sato T., et al., *Physica E: Low-dimensional Systems and Nanostructures*, Volume 40, 1495-1497 (2008).
- [66]. B. H. Hong, "Synthesis and applications of graphene for flexible electronics" *Graphene 2011 at Imagine nano* (2011).
- [67]. Kakani S.L., and Kakani A., "Material Science", SBN (13): 978-81-224-2656-4 (2004).
- [68]. *Products Catalog, Total Solution for Advanced Materials Research*, MTI, USA (2000).
- [69]. *Operational Manual*, MTI Corporation, 19th Street, Richmond, CA 94804, USA (2000).
- [70]. Klug, H. P., and L. E. Alexander, "X-ray diffraction procedures for polycrystalline and amorphous materials", 2nd ed. Wiley, New York, (1974).
- [71]. Charles Kittel, "Solid State Physics", Wiley publishers 7th Edition (1996).
- [72]. Cullity B. D., "Elements of X-ray Diffraction", 2nd.Edition, Addison-Wesley, California, USA (1978).
- [73]. Manoj B., Kunjomana A.G., *Int. J. Electrochem. Sci.*, Volume 7, 3127– 3134 (2012).
- [74]. Burcu Saner, Firuze Okyay, Yuda Yürüm, *Fuel*, Volume 89, 1903–1910 (2010).
- [75]. Raziieh Jabari Seresht et al, *Applied Surface Science*, Volume 276, 672–681 (2013).
- [76]. Bozzola J. J., and Russell L. D., "Electron Microscopy", Jones and Bartlett Publishers Inc., Boston (1992).
- [77]. Heath J. P., "Dictionary of Microscopy", John Wiley & Sons Ltd., Chichester, England (2005).
- [78]. Flegler S. L., Heckman J. W. Jr. and Klomparens K. L., "Scanning and Transmission Electron Microscopy", W. H. Freeman and Company, New York (1993).
- [79]. Lickfeld K. G., "Elektronenmikroskopie", Eugen Ulmer Publisher, Stuttgart, Germany (1979).
- [80]. Haguenu F., Hawkes P. W., Hutchison J. L., Satiat-Jeunemaître B., Simon G. T. and Williams D. B., *Microscopy and Microanalysis*, Volume 9, 96 (2003).
- [81]. M. von Ardenne. Patent: Improvements in Electron Microscopes, (1937).
- [82]. Goldstein et al. *Scanning Electron Microscopy and X-ray Microanalysis* (1981).
- [83]. E. Ruska, G. Binnig, and H. Rohrer, Nobel Prize in Physics, (1986).
- [84]. Ferrari. A. C. et al. *Phys. Rev. Lett.*, Volume 97, 187401 (2006).
- [85]. Das, R.S. & Agrawal, Y. *Vibrational Spectroscopy*, Vol. 57(2), pp.163–176 (2011).
- [86]. "Raman spectroscopy basis" Princeton Instruments.
- [87]. Valentina Di Cristo., *Structural and electrical characterization of graphene after ion irradiation Master Thesis.*, Uppsala university Sweden, (2010).

- [88]. Widenkvist E. "PhD thesis: Fabrication and Functionalization of graphene and other carbon nanomaterials in solution", Uppsala University, (2010).
- [89]. Ferrari A.C., Meyer J.C., et al. *Physical Review Letters*, Volume 97, 187401-4 (2006).
- [90]. Jafri H. et al. *Journal of Physics*, Volume 43, 045404 (2010).
- [91]. Compagnini G. et al. *Carbon*, Volume 47(14), 3201-3207 (2009).
- [92]. Agilent Technologies, Inc.2001, Agilent 4284A Precision LCR Meter Operation Manual 8th edition Japan, Agilent Technologies, Inc.2000-2001
- [93]. Greg Amorese. LCR / Impedance Measurement Basics. Hewlett-Packard Company Kobe Instrument Division, California 95403 U.S.A.
- [94]. Agilent Technologies, Inc.2001, Agilent 4284A Precision LCR Meter Operation Manual 8th edition Japan, Agilent Technologies, Inc.2000-2001
- [95]. Agilent Technologies, Inc.2001, Agilent 4278A, Operation Manual, Agilent Technologies Corp.
- [96]. Impedance Measurement Handbook, Agilent Technologies Corp. Second Edition, (2001).
- [97]. Ohmsha, "Basics and Applications of Ceramic Capacitor", First Edition, (2003).
- [98]. Warren B.E., *Phys. Rev.*, Volume 59, 693-698 (1941).
- [99]. Cullity, B.D. *Elements of X-ray Diffraction* (Addison- Wesley Publishing Company Inc.: California: (1956).
- [100]. Jeong, H. K., et al., *Chem. Phys.Lett.*, Volume 470, 255-258 (2009).
- [101]. Warren B.E., *Phys. Rev.*, Volume 59, 693-698 (1941).
- [102]. Manoj B., Kunjomana A.G. *Int. J. Electrochem. Sci.*, Volume7, 3127- 3134 (2012).
- [103]. Burcu Saner, Firuze Okyay, Yuda Yürüm, *Fuel*, Volume 89, 1903-1910 (2010).
- [104]. Razieh Jabari Seresht et al, *Applied Surface Science*, Volume 276, 672-681 (2013).
- [105]. Ju, H. M.; Huh, S. H.; Choi, S. H. & Lee, H. L., *Mater. Lett*, Volume 64, 357-360 (2010).
- [106]. Hiten Sarma, Sarma K.C., *International Journal of Scientific and Research Publications*, Volume 4, Issue 3, (2014).
- [107]. Reference for Dielectric constant vs frequency plot a hump in graph.
- [108]. Ferrari C.A. *Journal of Solid State Chemistry*, Volume 143, 47-57 (2007).
- [109]. Nair, R. R. et al. *Science* 320, 1308-1308 (2008).
- [110]. Huang L, Chang Q H, Guo G L, Liu Y, Xie Y Q, Wang T, et al. *Carbon* ; Volume 50:551-6 (2012).

- [111]. Park H J, Meyer J, Roth S, Skakalova V. Carbon; Volume 48: 1088–94 (2010).
- [112]. Kim Y, et al. Appl. Phys.Lett., Volume 98, 263106–9 (2011).
- [113]. Yingpeng Wu, et al. Nano Res., Volume 3(9), 661–669 (2010).
- [114]. Tuinstra F., Koenig J. Journal of Chemical Physics, Volume 53, 1126–1130 (1970).
- [115]. Yoon D., Moon H., Che H. Journal of the Korean Physical Society, Volume 55, 1299–1303 (2009).
- [116]. Slonezewski J. C. and Weiss P. R., Phys. Rev., Volume 109, 272 (1958).
- [117]. Ku H. S., Siores E., Bull J. A. R. Journal of Microwave Power and Electromagnetic Energy, Volume 34(4), 195–205 (1999).
- [118]. Miles P. A., Westphal W. B., and A. Von Hippel. Reviews of Modern Physics, Volume 29(3), 279–307 (1957).
- [119]. Kooops C.G. Physical Review, Volume 83(1), 121–124 (1951).
- [120]. Mo C. M., Zhang L., and Wang G., Nanostruct. Mater. Volume 6, 823-826 (1995).
- [121]. Anilkumar K. R., Parveen A., Badiger G. R., Ambika Prasad M. V. N., Physica, Volume 404, 1664 (2009).
- [122]. Jeong, H. Y. et al. Nano Lett. Volume 10, 4381–4386 (2010).
- [123]. Ramesh Patil, et al. J. App. Poly. Sci; Volume 121, 262 (2011).
- [124]. Patil A.N., et al. Mater. Sci., Volume 23(5), 361 (2000).
- [125]. Fang H., et al. Phys. Status Solidi, Volume 192, K11, (1995).
- [126]. R. H. Telling et al. Nat. Mater., Volume 2, 333–337 (2003).
- [127]. D. Wang, et al. Polymer, Volume 54, 1916–1922 (2013).
- [128]. A. Dey, S. De, A. De, S.K. De, Nanotechnology, Volume 5, 1277(2004).
- [129]. H. Elim,W. Ji, A.H. Yuyono, J.M. Xue, J. Wang, Appl. Phys. Lett. Volume 82, 2691(2003).
- [130]. Y.S. Yeh, J.T. Lue, Z.R. Zheng. IEEE Trans. Volume 53 1756(2005).
- [131]. A.Thakur, P.Thakur, J.H.Hsu, Journal of Alloys and Compounds. Volume 509, 5315 (2011).
- [132]. J.Y. Kim, et al. Adv. Mater., Volume 25, 2308–2313(2013).
- [133]. Wagner K. W., Amer.Phys, Volume 40, 137 (1973).
- [134]. Anilkumar K. R., Parveen A., Badiger G. R., Ambika Prasad M. V. N., Physica, Volume 404, 1664 (2009).
- [135]. Jeong, H. Y. et al. Nano Lett. Volume 10, 4381–4386 (2010).
- [136]. Earthana F et al. Phys. Stat. sol., Volume 104, 793 (1987).

- [137]. Khetre S. M et.al. *Advances in Applied Science Research*, Volume 2 (4):503-511(2011).
- [138]. Pollak M., *Phil. Mag.*, Volume 23,519 (1971).
- [139]. Elliot S. R. *Solid State Commun*, Volume 28, 145 (1978).
- [140]. Lahiri, J.; Lin, Y.; Bozkurt, P.; Oleynik, I. I.; Batzill, M. *Nat. Nanotechnol.*, Volume 5, 326–329 (2010).
- [141]. Yazyev, O. V.; Louie, S. G. *Nat. Mater.* Volume 9, 806–809 (2010).
- [142]. Kim, K.; Lee, Z.; Regan, W.; Kisielowski, C.; Crommie, M. F.; Zettl, A. *ACS Nano*, Volume 5, 2142–2146 (2011).
- [143]. Song, H. S.; S. L. Li, S. L.; Miyazaki, H.; Sato, S.; Hayashi, K.; Yamada, A.; Yokoyama, N.; Tsukagoshi, K. *Sci. Rep. 2*, 337; DOI:10.1038/srep00337(2012).
- [144]. S H M Jafri et al. *J. Phys. D: Appl. Phys.* Volume 43, 045404 (2010).
- [145]. M. Hashim, Alimuddin, S. Kumar, S. E. Shirsath, R. K. Kotnala, J. Shah and R. Kumar, *Materials Chemistry and Physics*, Volume 139, 364 (2013).
- [146]. M. Naeem, N. A. Shah, I. H. Gul and A. Maqsood, *Journal of Alloys and Compounds*, 487, 739 (2009).

7 TURNITIN REPORT

Influences of Thermal Annealing on Physical Properties of Graphene Nanoplatelets by
Muhammad Akhtar

From BS, MS and PhD Thesis (BS, MS, Ph.D Thesis Plagiarism)

Processed on 22-Oct-2015 09:16 PKT

ID: 588392501

Word Count: 12708

Similarity Index: 6%

Similarity by Source

Internet Sources: 1%

Publications: 4%

Student Papers: 3%

sources:

1

1% match (publications)

Koshino, Mikito. "Stacking-dependent optical absorption in multilayer graphene", New Journal of Physics, 2013.

2

< 1% match (student papers from 19-Feb-2015)

Submitted to University of Pune on 2015-02-19

3

< 1% match (publications)

Afroze, Tamanna, and A. H. Bhuiyan. "Alternating Current Electrical Properties of Thin Films of Plasma Polymerized 1, 1, 3, 3-Tetramethoxypropane", Advances in Polymer Technology, 2014.

4

< 1% match (student papers from 28-May-2014)

Submitted to IIT Delhi on 2014-05-28

5

< 1% match (student papers from 20-Jun-2012)

Submitted to Higher Education Commission Pakistan on 2012-06-20

6

< 1% match (Internet from 06-Jan-2015)

<http://en.m.wikipedia.org/wiki/Carbon>

7

< 1% match (publications)

S. P. Mahapatra. "Dynamic mechanical and dielectric relaxation characteristics of microcellular rubber composites", Polymers for Advanced Technologies, 09/2008

8

< 1% match (Internet from 22-Oct-2011)

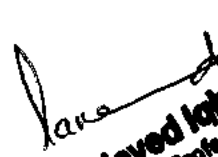
http://www.cmdmc.com.br/redecmdmc/lab/arquivos_publicacoes/3402_In2O3%20microcrystals%20obtained%20from%20rapid%20calcination.pdf

9

< 1% match (publications)

Heimann, Robert B., and Hans D. Lehmann. "Characterisation and Testing of Bioceramic Coatings", Bioceramic Coatings for Medical Implants, 2015.

10


Dr. Javed Iqbal Saggu
Assistant Professor (Physics)
International Islamic University
Islamabad.

< 1% match (student papers from 30-Jan-2015)
Submitted to King's College on 2015-01-30
11

< 1% match (publications)
Zhang, X.W.. "Synthesis and structure of nitrogenated tetrahedral amorphous carbon thin films prepared by a pulsed filtered vacuum arc deposition", *Diamond & Related Materials*, 200301
12

< 1% match (student papers from 09-Dec-2014)
Submitted to Higher Education Commission Pakistan on 2014-12-09
13

< 1% match (student papers from 17-Aug-2015)
Submitted to Kumoh National Institute of Technology Graduate School on 2015-08-17
14

< 1% match (student papers from 29-Jul-2015)
Submitted to Higher Education Commission Pakistan on 2015-07-29
15

< 1% match (publications)
Shi, Xiaomei, Jingdai Wang, Binbo Jiang, and Yongrong Yang. "Influence of nanofiller dimensionality on the crystallization behavior of HDPE/carbon nanocomposites", *Journal of Applied Polymer Science*, 2013.
16

< 1% match (publications)
Ravinder, D.. "High-frequency dielectric behaviour of gadolinium substituted Ni-Zn ferrites", *Materials Letters*, 200104
17

< 1% match (student papers from 25-Mar-2013)
Submitted to University of Nottingham on 2013-03-25
18

< 1% match (student papers from 02-May-2012)
Submitted to Nanyang Technological University, Singapore on 2012-05-02
19

< 1% match (student papers from 02-Aug-2010)
Submitted to University of California, Los Angeles on 2010-08-02
20

< 1% match (publications)
Lisa Vaccari. "Carbon Nanotubes", *NanoScience and Technology*, 2007
21

< 1% match (student papers from 18-Aug-2015)
Submitted to Institute of Graduate Studies, UiTM on 2015-08-18
22

< 1% match (publications)
Variankaval, Narayan. "X-Ray Methods", *Analytical Instrumentation Handbook Second Edition*, 2004.
23

< 1% match (student papers from 05-Feb-2014)
Submitted to Jamia Milia Islamia University on 2014-02-05
24

< 1% match (student papers from 09-Jan-2014)
Submitted to Higher Education Commission Pakistan on 2014-01-09

25

< 1% match (student papers from 11-Jul-2014)

Submitted to Jawaharlal Nehru Technological University on 2014-07-11

26

< 1% match (Internet from 05-Nov-2014)

http://202.127.207.43/bitstream/334002/12274/1/Preparation%20of%20porous%20flower-like%20CuO_ZnO%20nanostructures%20and%20analysis%20of%20their%20gas-sensing%20property.pdf

27

< 1% match (Internet from 25-Nov-2009)

<http://lib.zjnu.net.cn/lunwenshoulu/qingkuang/ei/2009%E5%B9%B4EI%20Compendex%E6%94%B6%E5%BD%95%E6%B5%99%E6%B1%9F%E5%B8%88%E8%8C%83%E5%A4%A7%E5%AD%A6%E8%AE%BA%E6%96%87141%E7%AF%87.pdf>

28

< 1% match (Internet from 21-Feb-2015)

<http://www.doria.fi/bitstream/handle/10024/102210/Pulsed%20electric%20field%20assisted%20sol-gel%20preparation%20of%20TiO2%20particles%20and%20their%20photocatalytic%20properties.pdf?sequence=2>

29

< 1% match (publications)

Liming Dai. "Carbon Nanomaterials for Advanced Energy Conversion and Storage", Small, 04/23/2012

30

< 1% match (Internet from 05-Dec-2011)

http://public.iscpif.fr/~cointet/nano/nano/2010/WoSRecords_7_3001_3500.txt

31

< 1% match (publications)

Matis, Martin, Friedemann Tonner, Carsten Glanz, and Ivica Kolaric. "Electrochemical Exfoliation: : A Cost-Effective Approach to Produce Graphene Nanoplatelets in Bulk Quantities", Graphite Graphene and Their Polymer Nanocomposites, 2012.

32

< 1% match (publications)

Lai, King Wai Chiu, Carmen Kar Man Fung, Hongzhi Chen, Ruiguo Yang, Bo Song, and Ning Xi. "Fabrication of graphene devices for infrared detection", 2010 IEEE Nanotechnology Materials and Devices Conference, 2010.

33

< 1% match (student papers from 06-Mar-2013)

Submitted to Higher Education Commission Pakistan on 2013-03-06

34

< 1% match (Internet from 06-Feb-2004)

<http://notes.chem.usyd.edu.au/course/george/Chem1102/intro.pdf>

35

< 1% match (publications)

You Jing-Han. "Fifth-Nearest-Neighbor Tight-Binding Description of Electronic Structure of Graphene", Communications in Theoretical Physics, 06/2010

36

< 1% match (Internet from 01-Mar-2015)

<http://etd.uovs.ac.za/ETD-db/theses/available/etd-08042014-122410/unrestricted/TshabalalaMA.pdf>

37

< 1% match (Internet from 21-Jun-2006)

<http://www.apsidium.com/elements/078.htm>

38

< 1% match (publications)

M. S. Aziz. "Electrical Conductivity and Dielectric Properties of Bulk Glass V2O5 (ZnO, PbO) SrO FeO", Physics Research International, 2011

39

< 1% match (publications)

Shaikh, A.. "Temperature and frequency-dependent dielectric properties of Zn substituted Li-Mg ferrites", Journal of Magnetism and Magnetic Materials, 199905

40

< 1% match (publications)

E. T. Yu. "Local Polarization Effects in Nitride Heterostructures and Devices", Polarization Effects in Semiconductors, 2008

41

< 1% match (publications)

Chen, Xiu Fang, Ru Sheng Wei, Yu Qiang Gao, Yan Peng, Sheng Song, Li Huan Wang, Xiao Bo Hu, Xian Gang Xu, and Min Hua Jiang. "Growth of Wafer Size Graphene on SiC Substrates", Materials Science Forum, 2011.

42

< 1% match (publications)

Kim, Sunghwan, and Jin Yu. "Recrystallization-induced void migration in electroplated Cu films", Scripta Materialia, 2012.

43

< 1% match (publications)

Shmavonyan, G. Sh.; Sevoyan, G. G. And Aroutiounian, V. M.. "Enlarging the surface area of monolayer graphene synthesized by mechanical exfoliation", Armenian Journal of Physics,

2013.